Study of titanium alloy Ti6242S oxidation behaviour in air at 560°C: Effect of oxygen dissolution on lattice parameters

M. Berthaud, I. Popa, R. Chassagnon, O. Heintz, J. Lavková, S. Chevalier

Version of Record: https://www.sciencedirect.com/science/article/pii/S0010938X19300617
Manuscript_954a7b0a3d41fe85e614e898e2cbc7f2

Study of titanium alloy Ti6242S oxidation behaviour in air at 560°C: effect of oxygen dissolution on lattice parameters

M. Berthaud*[1], I. Popa[1], R. Chassagnon[1], O. Heintz[1], J. Lavková[2], S. Chevalier[1]

[1] *ICB, UMR 6303CNRS-Université de Bourgogne, 21078 Dijon Cedex, France*

[2] *Department of Surface and Plasma Science, Charles University, V Holešovičkách 2, 18000 Prague 8, Czech Republic*
** maxime.berthaud@u-bourgogne.fr*

Abstract

High temperature oxidation of titanium alloy Ti6242S was studied in air at 560°C up to 10000 hours. Oxidation kinetics obeys a parabolic law (k_p = 8.7 x 10^{-15} $g^2.cm^{-4}.s^{-1}$). Oxygen dissolution in the metal was found to represent between 80 and 90% of the total mass gain. Thin oxide scales are mainly composed of TiO_2, in top of which some alumina is present. Titanium nitride was detected as a very thin layer at the outer part of the metallic substrate. Underneath, the oxygen dissolution area was found to reach the maximum brittleness after 1000 hours of oxidation.

Highlights

- Oxidation of Ti6242S alloy at 560°C in air follows a parabolic kinetics law.
- Oxide growth and oxygen dissolution kinetics obey to parabolic laws.
- Oxide scales are thin and mainly composed of rutile and anatase.
- Nitrogen enrichment of a thin layer in the metal.
- Oxygen dissolution in the metal results in lattice dilatation.

Keywords

A. Titanium
A. Alloy
B. TEM
B. X-ray diffraction
C. High temperature corrosion

Introduction

Titanium and its alloys are generally used in industrial applications when light materials are required, such as energy production, chemical industry or aeronautics [1–7]. Pure titanium has hexagonal close-packed (hcp) structure, called α-phase, at temperatures below 882°C and body-centered cubic (bcc) structure, called β-phase, at temperatures above 882°C. In the case of titanium alloys, both α and β phases can be stabilised at room temperature, by addition of α- and β-stabilising elements, respectively.

Thermal oxidation of titanium alloys leads to the simultaneous formation of an oxide scale at the surface of the specimen and dissolution of oxygen in the bulk [8]. Oxide growth during thermal oxidation of titanium alloys takes place through anionic diffusion mechanism [9]. A continuous oxide layer is formed after the first stages of oxidation. Then O^{2-} ions diffuse through the oxide layer to oxidise metallic titanium. In parallel with the oxide scale growth, oxygen dissolution equally takes place as α-phase of titanium presents high oxygen solubility. Up to 33 at.% of oxygen may dissolve in interstitial sites of α-titanium [10–12]. In contrast, oxygen dissolution in β-phase of titanium is very limited [13].

Titanium hcp phase lattice parameters are modified by oxygen dissolution [14]. Octahedral sites of α-Ti host lattice are occupied by interstitial oxygen atoms [14–17], leading to an anisotropic deformation of the hcp cell. Both ***a*** and ***c*** lattice parameters are impacted by the increase of oxygen concentration. However, ***a*** parameter shows very little variation, while ***c*** parameter and ***c***/***a*** ratio present a rather important increase when oxygen content varies from 0 up to 33 at.% [11,14,17].

Oxygen dissolution in α-titanium has an important effect on the mechanical properties of the material. Tensile tests show that ductility decreases with oxygen concentration [18–27]. Dubertret [26] showed that interstitial oxygen leads to total suppression of plastic deformation modes in the metal at room temperature, and finally to brittle fracture. The hardening effect of oxygen dissolution makes microhardness measurement a good technique to evaluate oxygen dissolution depth [18,19,28–31].

The use of Ti alloys allows decreasing the reaction kinetics and oxygen dissolution phenomena as compared to pure titanium [32]. Titanium alloy Ti-6Al-4V (TA6V) is largely used in industrial applications. Its behaviour in air at high temperature is largely reported in the literature, showing that its use is limited below 400°C [6]. High-performance titanium alloys as Ti-6Al-2Sn-4Zr-2Mo-0.1Si (Ti6242S) were then developed, as they present lower reactivity and can be employed up to 550-600°C [7].

Several authors have studied the high temperature behaviour of titanium alloy Ti6242S in air. For temperatures between 500°C and 650°C, the weight gains of Ti6242S alloy follow a parabolic rate law [10,29,33,34]. The corresponding oxide layer thicknesses are reported to be very small and does not overcome 3.5 µm after 500 hours at 650°C [10,29,35]. The corrosion scales are composed of TiO_2 as rutile and anatase, but presence of Al and Zr was equally observed [10,35]. Oxygen dissolution depth in Ti6242S alloy increases with the temperature and presents parabolic dependence with the oxidation time between 500 and 700°C [10,29,33].

Nitrogen contained in the atmosphere may play an important role on the oxidation of titanium alloys during exposure to atmospheric air. Chaze *et al.* [36] observed that binary Ti alloys present lower oxidation kinetics in air at temperatures between 500°C and 700°C, as compared to a nitrogen-free atmosphere with the same O_2 partial pressure. The authors consider that nitrogen modifies the oxidation of titanium by accumulating at metal/oxide interface. Oxide scale adhesion was also improved in nitrogen-containing atmosphere. Similar observations were made on Ti6242S alloy behaviour. Dupressoire *et al.* [35] report a decrease of the oxidation kinetics and of the oxygen dissolution depth at 650°C in presence of nitrogen. Corrosion products appeared thinner and more compact.

The purpose of this work is to go deeper in the study of the oxidation of Ti6242S alloy. Isothermal exposures were performed at 560°C in air for durations up to 10000 hours. Corrosion scales were

characterised by means of scanning and transmission electron microscopy (SEM, TEM), X-rays diffraction (XRD) and X-ray photoelectron spectroscopy (XPS). The oxygen dissolution in the bulk was followed by microhardness measurements. Oxygen dissolution effect on cell parameters of the substrate was studied by Rietveld refinement of XRD patterns. Finally, the reaction rates corresponding to oxygen dissolution and to oxide formation will be extracted from the total weight gain.

Material and techniques

Table 1 gives the chemical composition of titanium alloy Ti6242S used in this study. It is a near-α titanium alloy, which contains less than 5% of β-phase. It has bimodal microstructure (also called duplex microstructure) composed of globular α grains and of lamellar α/β grains. The average size of globular α grains is of 10.1 ± 1.7 µm. Inside lamellar grains, α and β lamellas are 1.0 ± 0.4 µm and respectively 0.2 ± 0.1 µm wide. The grains size values are similar in different perpendicular cuts of the alloy, it can then be assumed as being isotropic.

Specimens were parallelepipeds of 20 mm x 10 mm x 2 mm. They were mechanically polished on SiC papers up to P600 grade, and then cleaned in ethanol using an ultrasonic bath. The dimensions of the parallelepipeds were measured and then their total area was calculated. Specimens were weighted using a Mettler Toledo balance with 0.1 mg accuracy.

The samples were oxidised in a muffle furnace in laboratory air at 560°C for times up to 10000h. In complement with these long-term experiments, short thermogravimetric tests were done for 100h. Experiments under synthetic air flow (120 mL/min) were performed with Setaram Setsys Evolution device for 100 hours, with a temperature ramp of 10°C/min up to 560°C.

Microstructural surface and cross-section characterisations were performed using JEOL JSM-7600F scanning electron microscope equipped with field emission gun (FEG). Chemical analyses were done by energy dispersive X-ray spectrometry (EDS). Data obtained were analysed using INCA software, provided by Oxford Instruments.

For better insight, transmission electron microscopy (TEM) analyses were performed on cross-section of the samples, by using a JEOL 2100 LaB_6 microscope, equipped with EDS analyser (EDX JEOL JED 2300T). In this purpose, thin cross-sections were previsoulsy prepared using focussed ion beam (FIB) technique.

Combining SEM-EDS oxygen distribution with microhardness profiles performed on cross section of the oxidised samples allowed following the oxygen dissolution in the bulk of the titanium alloy. Microhardness measurements were done with Zwick Roell ZHµ equipment under 25 grams load. The indentation prints have diagonal average values between 7.0 and 11.5 µm. These values are comparable to globular α grains size, but is lower that the size of α/β lamellar grains. The distance of the prints with respect to the metal surface was measured with an optical microscope.

The crystallographic phases present in the oxide scales grown on the aged samples were determined by X-ray diffraction analyses. The used diffractometer is a Brüker D8 Discover device using monochromatic Cu K_α radiation ($\lambda_{K\alpha1}$ = 0,154156 nm) and equipped with LYNXEYE detector. The incidence angle was fixed to 2° for all the experiments, corresponding to a penetration depth

of X-rays into the sample ~~(oxide scale and Ti-O solid solution)~~ between 2 and 3 µm and providing the best compromise for simultaneous observation of the oxide scale and of Ti-O solid solution.

X-ray diffraction patterns were used for Rietveld refinement in order to determine the lattice parameter and to study their variations related to oxygen dissolution. Rietveld refinement was performed by using MAUD program [37]. The instrument resolution was calibrated with LaB_6 NIST powder standard. Popa's model [38] was used to represent anisotropic crystallites and microstrains. The texture of the sample was taken into account by using a spherical harmonic model.

Nitrogen presence inside the sample was tested by X-ray Photoelectron spectroscopy (XPS). X-ray source had a wavelength corresponding to Kα line of aluminium (1486.6 eV). Binding energies of peaks were calibrated with respect to C1S peak at 284.8 eV from the adventitious hydrocarbon surface contamination. In the bulk, peaks were calibrated with respect to Al2p peak (72.8 eV).

Results

1. Raw material

The bimodal microstructure of the raw Ti6262S alloy is presented in Figure 1a. Two types of grains can be observed: dark grey globular grains and light grey laths in a dark grey matrix. Dark grey regions contain a higher Al content and a lower Mo content than the nominal Ti6242S composition (Table 2). At the same time, light grey regions are Mo-enriched and Al-depleted. Zirconium, tin and silicon are equally distributed in both types of grains. It is well known that Al is α-stabiliser element, while Mo is β-stabiliser. In consequence, the dark grey regions were identified to correspond to α-phase of Ti6242S, while the light grey regions correspond to β-phase. The XRD pattern acquired on the raw Ti6242S material (Figure 1b) shows the presence of a major hcp (α) phase and a minor CC (β) phase, as expected for a near-α alloy.

The Rietveld refinement of the XRD pattern allowed determining the cell parameters of hcp-α and CC-β structures. The as-obtained values are indicated in Table 3. Cell parameters of both phases were equally calculated from electron diffraction patterns. Figure2a presents a TEM dark field image showing selected areas where diffraction patterns associated to α-phase (Figure 2b) and to β-phase (Figure2c) were acquired. Average values of the cell parameters were calculated over several areas selected on the sample. The as-obtained values are indicated in Table 3 and show a very good concordance between the two methods.

Table 3 equally indicates the cell parameters of Ti6242 α- and β-phases reported in the literature [17]; it shows a very good agreement with the present study. A comparison with pure Ti cell parameters [39] is equally made, showing similar ***c*** hcp parameter, but higher ***a*** hcp parameter; the presence of addition elements seems to influence only ***a*** hcp value. The comparison is difficult concerning the cell parameter of the cc structure, as it only exists above 882°C for pure titanium, while the results of the present study were obtained at room temperature.

Surface hardness of raw Ti6242S was measured by Vickers microhardness. An average made on 10 indentations gave a value of 375 ± 15 HV.

2. Oxidation kinetics at 560°C in laboratory air

Figures 3a and 3b present the surface mass gain of Ti6242S alloy versus the oxidation time at 560°C obtained by thermogravimetry in dry air up to 100 hours (Figure 3a) and in muffle furnaces in laboratory air for long exposure periods, up to 10000 hours (Figure3b). Both curves follow a parabolic rate law with time at this temperature. Associated k_p constants were calculated using the complete parabolic law given by the following equation [40]:

$$t = C_1 + C_2 \times \frac{\Delta m}{A} + \frac{1}{k_p} \times \left(\frac{\Delta m}{A}\right)^2 \qquad \text{Equation (1)}$$

where $\frac{\Delta m}{A}$ is the normalised mass gain per surface area of the samples and t is the oxidation time, while C_1 and C_2 are constants given by the fit of the experimental data.

The parabolic rate constant obtained during 100 hours exposure in dry air is $k_p = 1.4 \times 10^{-14}$ g².cm^{-4}.s^{-1}, while the value associated to long-term exposure in laboratory air is $k_p = 8.7 \times 10^{-15}$ g².cm^{-4}.s^{-1}. It can be noticed that the two values obtained are very close, in spite of different exposure times and environments.

3. Characterisation of the corrosion products

Figure 4 presents cross section SEM images of the samples aged for 1000, 6000 and 10000 hours in laboratory air at 560°C. The oxide scales are adherent to the metallic substrate. ~~Their thickness is increasing with the exposure time and is given in Table 4; the thicknesses are very low for all samples and do not overcome 700 nm after 10000 hours of exposure.~~ Their average thickness is given in Table 4. These values were obtained by measuring on cross-section SEM images at different locations of the samples. For each sample, 3 images were used and 5 measurements were done on each image. The thickness of the scales is increasing with the exposure time. However, the oxide scales remain very thin for all samples and do not overcome 700 nm after 10000 hours of exposure.

For all the samples, the corrosion scales are made of two parts. The inner part, which represents the majority of the scale, is multilayered and composed of Ti and O in proportions corresponding to TiO_2. At the metal/oxide interface, the first TiO_2 layer is compact; above this layer, porous TiO_2 layers are observed. The second part of the scale, situated at the interface with the atmosphere, is represented by a darker edging with needle-shaped morphology. The chemical contrast indicates that the nature of this outer part should be different from the inner one. However, the very low thickness of this edging did not allow precise identification of its composition.

In agreement with SEM-EDS results, XRD analyses showed that the oxide scale is mainly composed of TiO_2 rutile. TiO_2 anatase was also identified for times higher than 600 hours, in a proportion that increases with the oxidation time (Figure 5).

In order to obtain better insight on the composition of the oxide scale, TEM observations were done on Ti6242S FIB lamella extracted after oxidising the sample for 300 hours in laboratory air at 560°C. As previously observed by SEM for longer exposure periods, the oxide layer is extremely thin (about 50 nm), dense and compact (Figure 6a). TEM-EDS profiles acquired from the external interface up to a depth of 1µm inside the bulk of the sample are presented in Figure 6b. The data were previously smoothed with respect to Savitzky-Golay algorithm [41], with a polynomial function of 2nd degree and an interval of 5 points as variables. Smoothing the plot leads to an averaging of the measured content values, but gives a clear trend on their evolution. The oxygen content clearly evidences the zone corresponding to the oxide scale and that corresponding to the

metallic substrate. The content of α- and β-stabilising elements allows identifying α- and β-metallic grains, equally indicated on Figure 6a and Figure 6b.

At the outer oxide surface, Al, Ti and O are detected. When going deeper in the oxide layer, the Al signal vanishes and only Ti and O remain present. The elementary composition suggests that a very thin Al_2O_3 layer is present on top of TiO_2 phase.

At the metal/oxide interface, a high content of nitrogen is detected, on a very thin layer of less than 200 nm thickness. In this region, the oxygen content is rather low, less than 5-10 at.%. It seems that at the outer part of the metallic substrate, a nitrogen dissolution zone is formed instead of the expected oxygen dissolution area, which is located deeper in the metal. Indeed, nitrogen percentage decreases fast with the distance from the metal/oxide interface, together with an increase of oxygen content. Inside the oxygen dissolution area, the oxygen percentage slowly diminishes with the increasing depth of α-phase. However, its value is very close to zero when crossing β-grains (Figure 6a-b), in agreement with the low solubility of oxygen in β-phase.

In order to verify the presence of alumina at the outer part of the sample and to quantify more accurately nitrogen presence at the metal/oxide interface, XPS analyses were done on a sample oxidised for 100 hours. Successive sputtering sequences followed by XPS analyses were performed to reconstruct chemical profiles from the external surface to the metallic bulk (Figure 7). The resulting XPS elementary profiles are similar to those obtained by TEM-EDS, showing Al enrichment at the external oxide surface and N enrichment in the metal beneath the oxide scale.

The XPS spectrum acquired at the external surface of the sample reveals that Al 2p peak is located at 75.25 eV, while O 1s peak is located at 531.5 eV (Figure 9a-b). These binding energies allow confirming the presence of Al_2O_3 at the outer part of the oxide scale [42,43], as suggested previously by TEM-EDS analyses.

The nitrogen content present in the external part of the metal, near the metal/oxide interface (Figure 7) reaches up to 28 at.% and proves nitrogen presence suggested by TEM-EDS analysis. Moreover, at this location, Ti $2p_{1/2}$ and Ti $2p_{3/2}$ peaks found at 454.6 and 460.6 eV (Figure 9a) do not correspond to metallic titanium (of 454.1 eV [44,45] and 460.8 eV [44] respectively. Literature suggests that these binding energies might correspond to a titanium nitride phase [46,47]. Indeed, N1s binding energy determined in the present study is of 397.3 eV (Figure 9b), close to the value found by Onyiriuka et al. for TiN phase [48]. However, since the employed technique (i.e. successive sputtering) can favourably sputter N atoms as compared to Ti atoms. In consequence, Ti/N ratio measured experimentally might be artificially decreased. Titanium nitride may in reality be richer in Ti, like for instance Ti_2N phase.

4. Oxygen dissolution in α-Ti6242S

Oxygen dissolution in the alloy was studied by means of microhardness indentations coupled with SEM-EDS oxygen profiles measured on cross sections of the oxidised samples from the external interface to the bulk of the samples. The microhardness and oxygen dissolution profiles obtained on Ti6242S samples oxidised up to 10000 hours in laboratory air at 560°C are presented in Figure 10.

Very high micro-hardness values are obtained at the metal/oxide interface, between 620 $HV_{0.025}$ for the sample oxidised 1000 hours and 850 $HV_{0.025}$ for the sample exposed for 10000 hours. The hardness values quickly decrease in all cases to reach a plateau corresponding to the average value of the raw Ti6242S alloy (~375 $HV_{0.025}$) at distances from the interface that increase with the

oxidation time. The oxygen content presents a similar evolution, with a maximum value of about 27 at.% near the interface with the metal. It should be noted here that, because of oxygen surface pollution, the oxygen content measured by EDS is certainly over-evaluated of several at.%. Therefore, the oxygen content values shown in Figure 10 should not be taken as quantitative; nevertheless, the existence of oxygen concentration profiles is evident for all the samples.

The thickness of oxygen dissolution area is then obtained by combining microhardness and EDS oxygen profiles for each sample (Table 5). Its evolution against oxidation time is plotted on Figure 11a. A parabolic-like dependence between the thickness of oxygen dissolution area and oxidation time is shown, as confirmed by the plot of the oxygen dissolution depth versus the square root of the exposure time in Figure 11b.

The oxygen dissolution phenomenon was equally followed by monitoring the variation of hcp cell parameters of Ti6242S versus the oxidation time. A previous synchrotron diffraction study performed by Bailleux *et al.* on the whole thickness of the oxygen dissolution area [14] showed that the oxygen dissolution for given temperature and time leads to a linear correlation between c/a ratio of hcp structure with the oxygen content and microhardness. The experiments done in the present paper, at low fixed incidence angle, limit the X-rays penetration to the outer part of the oxygen dissolution area, corresponding to the highest oxygen content, and give complementary information to the study of Bailleux *et al.*

Figure 12 shows XRD patterns of Ti6242S samples obtained before and after different exposure periods (1000 hours, 3000 hours, 10000 hours) at 560°C in air. It can be noticed that, when comparing to the raw sample, the diffraction peaks of hcp phase are shifted toward lower 2θ angles after high temperature exposure, showing an increase of the cell volume related to the oxygen dissolution phenomenon. Moreover, the shift is increasing with the exposure time, suggesting an enhancement in time of the oxygen content dissolved at the outer part of the metal.

Figure 13 represents the evolution in time of ***a*** and ***c*** cell parameters of hcp Ti6242S structure, determined by Rietveld refinement. Both parameters increase with the exposure time. However, they present a rapid increase for short exposure times and seem to level after 1000 hours oxidation. Parameter ***c*** presents a much higher increase than parameter ***a***.

Since oxygen solubility in β-phase of Ti6242S alloy is very low [14,15,17], it can be assumed that CC cell modification by oxygen dissolution is negligible. Indeed, the Rietveld refinement of XRD patterns did not show any important evolution of the CC cell parameter with the oxidation time.

5. Dissociation of oxygen dissolution from oxide growth

Oxygen dissolution in α-phase of Ti6242S alloy simultaneously takes place with oxide formation. In order to have a better insight of each phenomenon, it is necessary to separate their contribution from the total measured weight gain. Since the amounts of alumina present in the oxide layer and nitrogen diffused inside the metal are very small, we assume that their impact on the total weight gain can be neglected. As a consequence, it can be considered that the total measured mass gain is the sum of contributions related to TiO_2 growth on one hand and to oxygen dissolution in the metallic substrate on the other hand.

The calculation, based on the measurement of the oxide scale thickness e_{TiO2} by SEM, gives access to the weight gain $\Delta m_{O2(TiO2)}$ related to oxygen uptake in the oxide layer, by assuming that the oxide layer is dense ($\rho_{ox} = \rho_{TiO2}$) and its thickness is constant:

$$\Delta m_{O2(TiO2)} = \frac{e_{TiO2} \times \rho_{TiO2} \times A \times M_{O2}}{M_{TiO2}} \qquad \text{Equation (2)}$$

The weight increase corresponding to oxygen dissolved in the metallic substrate can then be estimated, knowing the total weight gain of the sample and the oxygen weight contained in the oxide scale:

$$\frac{\Delta m_{O2(Ti-O\ solution)}}{A} = \frac{\Delta m_{tot}}{A} - \frac{e_{TiO2} \times \rho_{TiO2} \times M_{O2}}{M_{TiO2}} \qquad \text{Equation (3)}$$

with:
Δm_{tot} the total mass gain,
$\Delta m_{O2(TiO2)}$ the oxygen mass gain due to the oxide scale formation,
$\Delta m_{O2(Ti-O\ solution)}$ the oxygen mass gain induced by oxygen dissolution into the substrate,
e_{TiO_2} the thickness of the oxide layer,
ρ_{TiO_2} the density of rutile,
A the area of the specimen.

Because of the very thin corrosion products that form for low exposure times, oxide scale thicknesses could be measured by SEM only for oxidation times higher than 1000 hours. Corresponding weight gain due to oxide formation is plotted in Figure 14, as well as the resulting weight gain due to oxygen dissolution in the metal. Both weight gains follow parabolic kinetics laws with exposure time. Associated kinetic constants were calculated using the complete parabolic rate law [40] and found to be: $k_{p(\text{Oxygen dissolution})} = 6.0 \times 10^{-15}$ g^2.cm^{-4}.s^{-1} and $k_{p(\text{TiO2 formation})} = 3.7 \times 10^{-16}$ g^2.cm^{-4}.s^{-1}.

As in can be seen in Figure 14 and equally shown by the determined k_p values, oxygen dissolution in Ti6242S alloy at 560°C represents the major part of the total measured weight gain. However, the oxide scale plays an increasing role with exposure time Table 6.

Discussion

Two techniques were used to estimate the lattice parameters of α- and β-phase of titanium alloy Ti6242S, i.e. TEM electron diffraction and Rietveld refinement of XRD patterns. The results obtained, for hcp and CC structures, are very close to those obtained by Malinov *et al.* [17]. However, some differences can be noticed with respect to the cell parameters known for pure titanium. Indeed, if ***c*** parameter of hcp structure of the two materials are rather similar, parameter ***a*** is larger for pure titanium, in relation with alloying elements addition. Alloying elements are in this case metallic atoms, known to occupy Ti sites in substitution [9]. Aluminium is the main α-stabiliser dissolved in α-phase of Ti6242S alloy. However, neutral alloying elements such as Zr and Sn were also detected by EDS analysis of α-phase (see Table 1). Al atoms are slightly smaller than titanium atoms (r_{Al} =143 pm vs. r_{Ti} =147 pm [49]), whereas Zr and Sn atoms are larger (r_{Zr} = 160 pm and r_{Sn} = 158 pm [49]). However, the content of Zr and Sn present in α-phase of Ti6242S alloy is rather low (2 at.% and 0.8 at.%, as shown in Table 2). It can then be assumed

that the high content of Al (12.5 at.%) leads to a decrease of ***a*** cell parameter of α-phase as compared to pure Ti.

In contrast, comparison is much more difficult to make for CC structure, as β-phase of pure titanium only exists at temperatures higher than 882°C. Addition of β-stabiliser elements to titanium allows the stabilisation of a certain amount of β-phase at room temperature. Mo is the only β-stabiliser in Ti6242S alloy and its atomic radius is smaller than that of titanium (r_{Mo} =140 pm vs. r_{Ti} = 147 pm [49]), suggesting a diminishing of CC cell volume by alloying. Indeed, the unit cell parameter found for β-phase of Ti6242S alloy at room temperature (a = 3.261 Å) is smaller than β-Ti at 900°C (a = 3.307 Å [39]). However, this variation can equally be caused by the thermal dilatation of the cell when heating up to 900°C.

Oxidation process of the alloy was followed at 560°C and showed parabolic kinetic law. The parabolic rate constants were similar when determined from short time (100 h) thermogravimetric analysis (1.4×10^{-14} g².cm^{-4}.s^{-1}) or from long-term (10000 h) exposures (8.7×10^{-15} g².cm^{-4}.s^{-1}). These values are in good agreement with literature data on Ti6242S alloy [10,29,33,34,50]. Gaddam *et al.* [29] measured parabolic rate constants of 9.34×10^{-15} g^2.cm^{-4}.s^{-1} in air at 500°C and of 7.84×10^{-14} g^2.cm^{-4}.s^{-1} at 593°C. Dupressoire *et al.* [35] measured a parabolic kinetic constant equal to 1.9×10^{-13} g^2.cm^{-4}.s^{-1} in synthetic air at 650°C.

The kinetics constants were calculated by using the whole weight gain measured during the oxidation process. In this way, any separate information is not provided about the rates of oxide growth and oxygen dissolution. SEM cross section observations allow the measurement of oxide scales thicknesses and made possible the estimation of oxygen dissolution and oxide growth contribution to the global weight gain. Each phenomenon was found to follow parabolic kinetics rate laws; corresponding constants were then calculated: $k_{p(\text{Oxygen dissolution})} = 5.3 \times 10^{-15}$ g^2.cm^{-4}.s^{-1} and $k_{p(\text{TiO2 formation})} = 5.1 \times 10^{-16}$ g^2.cm^{-4}.s^{-1}. These results show that at 560°C, oxygen dissolution represents the largest part of the weight increase with time (approximately one order of magnitude higher than the oxide formation). In addition, it seems that the oxygen dissolution part decreases with the oxidation time. Indeed, oxygen dissolution represents 87% of the total weight gain after 1000 hours, and 79% after 10000 hours. Such values are in agreement with the study of Kofstad *et al.* [51] who measured a proportion of oxygen dissolution higher than 80% during the oxidation of pure titanium at 900°C for 30 minutes in air, in accordance with the very thin oxide scales they observed by SEM.

At 560°C, the oxide scales are very thin. They are composed of a dense TiO_2 layer at the metal/oxide interface surmounted by a second porous TiO_2 layer. At the outer part of the scale, a thin Al_2O_3 layer was detected by XPS and TEM-EDS analysis. Dupressoire *et al.* [35] observed comparable morphologies in synthetic air at 650°C. The structure of the oxide scale grown at Ti6242S surface can be understood on the basis of the mechanism proposed by Du *et al.* [52] in the case of Ti-6Al-4V alloy. Al_2O_3 and TiO_2 layers grow by outward diffusion of aluminium and inward diffusion of oxygen respectively. At early stages of oxidation, TiO_2 grows preferentially and once a thin TiO_2 layer is formed, alumina nucleates on top of it. At extended oxidation times, Al_2O_3 grows laterally and covers TiO_2. The layering of TiO_2 is in agreement with Stringer [53] and can be explained by the presence of high stresses in relation with a large Pilling-Bedworth (PPB) ratio in the Ti/TiO_2 system (R_{PB} = 1.7 [35]). The stress relaxation when a critical value is reached leads to cracks and gaps at the oxide/metal interface, which allow the formation of new TiO_2 layers.

The presence of nitrogen at the oxide/metal interface showed by EDS-TEM analyses was confirmed by XPS in a content that reaches 28 at.%. A thin N-rich layer is located between the oxide layer and the oxygen dissolution area. This observation is in agreement with the work of Göbel *et al.* [54]. Chaze *et al.* [36] outlined the beneficial effect of nitrogen-containing atmospheres on the oxidation rate of pure titanium and binary alloys of titanium (Ti-Al, Ti-Cr, Ti-Si) as compared to pure oxygen atmosphere. They observed important changes on the oxide scale morphologies depending on the presence of nitrogen. In pure O_2, the oxide scales were very stratified and porous whereas in air the oxide layers were thin and compact. The oxide also presented higher adherence to the substrate in presence of nitrogen. According to the authors, the higher diffusion coefficient of N than of O in rutile [55], coupled with a slower diffusion of nitrogen in the metal than oxygen [54,56–58], leads to an accumulation of nitrogen at the oxide/metal interface. If nitrogen occupies anionic vacancies in the oxide, this would decrease the driving force for the oxygen diffusion in rutile and therefore the oxidation kinetics. Nitrogen dissolved in the metal may also reduce the oxygen concentration at the interface and then may slow down oxygen ingress in Ti–O solid solution by occupying some of the reactional sites [36,59].

Recent work of Dupressoire *et al.* [35] confirmed the beneficial effect of nitrogen on titanium alloy Ti6242S at the temperature of 650°C. After exposure under 20%O_2-80%N_2, the oxide scale is 6 times thinner than after oxidation in 20%O_2-80%Ar. It is equally compact, in contrast to a multilayered porous and undulated layer grown in O_2-Ar.

According to Ti-N phase diagram, nitrogen solubility in α-Ti is around 4 at.% at 560°C [60]. For higher nitrogen contents (up to 33 at.%), titanium nitride Ti_2N should be formed. Nitrogen and titanium contents shown in the present study by XPS analysis (28 at .% and 56 at.%) suggest the existence of Ti_2N phase after 100 hours oxidation of Ti6242S alloy at 560°C. However, the sputtering technique used to acquire in-depth elementary percentages lead to a sub-evaluation of nitrogen content and does not allow to firmly confirm the existence of Ti_2N phase or to propose instead a N-richer phase like TiN. Ti_2N phase identification by other methods is difficult; for instance, XRD is not appropriate since diffraction peaks of titanium nitride are superposed to α-Ti peaks.

As it can be seen on TEM-EDS analyses (Figure 6a and 6b), oxygen dissolution occurred beneath the nitrogen-enriched layer. Oxygen dissolution was studied by coupling SEM-EDS profiles and microhardness measurements. The dissolution area thicknesses measured after different exposure periods at 560°C are in agreement with those reported in the literature for Ti6242S alloy. For an oxidation time of 500 hours, Gaddam *et al.* [29,33] observed a dissolution area of 10 µm at 500°C and 30 µm at 593°C. Oxygen dissolution area was 50 µm thick after a treatment of 1000 hours at 600°C, according to Baillieux *el al.* [28]. Moreover, oxygen dissolution depth was found to be parabolic dependant with the oxidation time (Figure 11). This observation is conform to literature data between 500 and 1000°C on Ti6242S alloy [10,29,33] and pure Ti [53,61] up to 500 hours. It can be noted that the oxygen content at the outer part of the metal, shown by SEM-EDS profiles, is lower than theoretical solubility of oxygen in pure α-Ti (Figure 10). This observation is in accordance with the paper of Shenoy *et al.* [22] who observed a reduction of oxygen solubility in α-phase of titanium alloy Ti6242S as compared to α-Ti. They attributed this maximum solubility decrease to the presence of alloying elements within the alloy.

Baillieux *et al.* [14] studied by synchrotron diffraction the effect of oxygen dissolution on the crystalline cell parameters of α-Ti. Lattice cell parameters of the hcp phase of pure titanium were

measured at different points inside the metal after oxidation in air at 700°C. They measured a small increase of ***a*** cell parameter together with a significant increase of ***c*** parameter at the outer part of the metallic substrate, leading to an increase of ***c/a*** ratio. Deep in the substrate, the values of ***a*** and ***c*** parameters were found to be similar to those of α-Ti lattice. Andersson *et al.* [11] and Kofstad *et al.* [51] made similar observations. In their studies, ***c/a*** ratio of the TiO_x compounds was increasing with oxygen content until 35% O_2. According to Baillieux *et al.* [14], the ***c/a*** ratio evolution for oxygen contents between 0 and 35at.% shows the hcp lattice expansion mostly along the c axis with oxygen dissolution. The authors also conclude that oxygen atoms occupy octahedral sites of α-Ti.

In the present study, the impact of oxygen dissolution on the lattice parameters of α-Ti6242S phase was followed by Rietveld refinement of XRD patterns registered after different oxidation tests. The low fixed angle diffraction technique provides data corresponding to the outer part of the oxygen dissolution area where maximum oxygen content is reached. The cell expansion upon oxygen dissolution takes place only along ***c***-axis, in agreement with the literature, confirming that oxygen diffusion and dissolution in hcp host lattice takes place through octahedral sites [14–17]. Once all the available sites are occupied by oxygen atoms, oxygen maximum solubility in α-phase is reached. The leveling after 1000 hours for ***c*** and ***c***/***a*** is interpreted as the necessary time to saturate the outer part of the dissolution area, or the time to reach the maximum embrittlement at the alloy surface. If taking into account that ***c*** parameter of Ti6242S is identical to that of pure Ti, it is possible to use the data of Andersson *et al.* [11] and Kofstad *et al.* [51] in order to determine the oxygen content corresponding to the largest value of ***c*** parameter obtained in this study. It would result that the maximum oxygen solubility in Ti6242S alloy corresponds to 25 at.%, instead of 33 at.% for pure Ti. This observation is in agreement with EDS-SEM elementary analysis (Figure 10) and with the study of Shenoy *et al.* showing that the oxygen dissolution in Ti6242S grade is diminished by the presence of alloying elements [22].

Conclusion

Oxidation of titanium alloy Ti6242S was studied in air at 560°C. A particular attention has been given to oxygen dissolution in the metal and its effects on the α-phase of the alloy. The following conclusions can be drawn from this work:

(1) Oxidation of titanium alloy Ti6242S at 560°C in air follows a parabolic kinetic law. Associated parabolic kinetics constant is 8.7×10^{-15} $g^2.cm^{-4}.s^{-1}$.
(2) Both oxide growth and oxygen dissolution kinetics obey to parabolic laws. Oxygen dissolution in α-Ti6242S is an order of magnitude faster than oxide growth ($k_{p(\text{Oxygen dissolution})} = 6.0 \times 10^{-15}$ $g^2.cm^{-4}.s^{-1}$ and $k_{p(TiO2\ \text{formation})} = 3.7 \times 10^{-16}$ $g^2.cm^{-4}.s^{-1}$.) but its part decreases with the oxidation time.
(3) Oxide scales are mainly composed of rutile and anatase. A thin alumina layer formed at the outer part of the oxide scale.
(4) Nitrogen presence at the outer part of Ti6242S alloy was shown by XPS and EDS-TEM analyses.
(5) Oxygen dissolution phenomenon was characterized as a function of the exposure time by combining microhardness and EDS-TEM oxygen content profiles.
(6) Complementary information on the dissolution process was provided by Rietveld refinement of XRD patterns acquired after different exposure times. A leveling occurs after 1000 hours of exposure. The corresponding oxygen solubility is lower than for pure Ti, due to the presence of alloying elements.

Data availability

The raw data required to reproduce these findings cannot be shared at this time due to technical or time limitations.
The processed data required to reproduce these findings cannot be shared at this time due to technical or time limitations.

Acknowledgements

This work was financially supported by the ICB laboratory. The authors would also like to thank Daniel MONCEAU for productive discussions and Frédéric HERBST and Nicolas GEOFFROY for technical support.

References

[1] B. Liu, J.-B. He, Y.-J. Chen, Y. Wang, N. Deng, Phytic acid-coated titanium as electrocatalyst of hydrogen evolution reaction in alkaline electrolyte, Int. J. Hydrog. Energy. 38 (2013) 3130–3136. doi:10.1016/j.ijhydene.2012.12.099.
[2] N.M. Kablaoui, S.L. Buchwald, Reductive cyclization of enones by a titanium catalyst, J. Am. Chem. Soc. 117 (1995) 6785–6786.
[3] N. Kashiwa, J. Yoshitake, The influence of the valence state of titanium in MgCl2-supported titanium catalysts on olefin polymerization, Makromol. Chem. 185 (1984) 1133–1138.
[4] J.M. Fraile, J.I. García, J.A. Mayoral, E. Vispe, Silica-supported titanium derivatives as catalysts for the epoxidation of alkenes with hydrogen peroxide: A new way to tuneable catalytic activity through ligand exchange, J. Catal. 189 (2000) 40–51.
[5] E. Efzan, M. Noor, S. Kesahvanveraragu, Review on Pipelines in Offshore Platform Processing System, Appl. Mech. Mater. 695 (2015) 684–687. doi:10.4028/www.scientific.net/AMM.695.684.
[6] C. Leyens, M. Peters, Titanium and titanium alloys, Wiley Online Library, 2003.
[7] R.R. Boyer, An overview on the use of titanium in the aerospace industry, Mater. Sci. Eng. A. 213 (1996) 103–114. doi:10.1016/0921-5093(96)10233-1.
[8] P. Kofstad, K. Hauffe, H. Kjollesdal, Investigation on the oxidation mechanism of titanium, Acta Chem. Scand. 12 (1958) 239–266.
[9] G. Lütjering, J.C. Williams, Titanium: Engineering Materials and Processes, Springer, Verlag Berlin, 2007.
[10] K.S. McReynolds, S. Tamirisakandala, A Study on Alpha-Case Depth in Ti-6Al-2Sn-4Zr-2Mo, Metall. Mater. Trans. A. 42 (2011) 1732–1736. doi:10.1007/s11661-011-0710-3.
[11] S. Andersson, B. Collen, U. Kuylenstierna, A. Magnéli, Phase analysis studies on the titanium-oxygen system, Acta Chem Scand. 11 (1957) 1641–1652.
[12] P. Kofstad, High Temperature Corrosion, Elsevier Applied Science, New-York, 1988.
[13] C.J. Rosa, Oxygen diffusion in alpha and beta titanium in the temperature range of 932° to 1142°C, Metall. Trans. 1 (1970) 2517–2522. doi:10.1007/BF03038377.
[14] J. Baillieux, D. Poquillon, B. Malard, Observation using synchrotron X-ray diffraction of the crystallographic evolution of α-titanium after oxygen diffusion, Philos. Mag. Lett. 95 (2015) 245–252. doi:10.1080/09500839.2015.1014876.
[15] M.A. Hongyan, M. Wang, W. Wu, Oxygen permeation behaviors and hardening effect of titanium alloys at high temperature, J Mater Sci Technol. (2004) 719–723.
[16] M. Dechamps, A. Quivy, G. Baur, P. Lehr, Influence of the distribution of the interstitial oxygen atoms on the lattice parameters in dilute H.C.P. titanium-oxygen solid solutions (90–4000 ppm at), Scr. Metall. 11 (1977) 941–945. doi:10.1016/0036-9748(77)90243-5.

[17] S. Malinov, W. Sha, Z. Guo, C.C. Tang, A.E. Long, Synchrotron X-ray diffraction study of the phase transformations in titanium alloys, Mater. Charact. 48 (2002) 279–295. doi:10.1016/S1044-5803(02)00286-3.
[18] K.S. Chan, M. Koike, B.W. Johnson, T. Okabe, Modeling of Alpha-Case Formation and Its Effects on the Mechanical Properties of Titanium Alloy Castings, Metall. Mater. Trans. A. 39 (2007) 171–180. doi:10.1007/s11661-007-9406-0.
[19] C. Leyens, M. Peters, D. Weinem, W.A. Kaysser, Influence of long-term annealing on tensile properties and fracture of near-α titanium alloy Ti-6Al-2.75Sn-4Zr-0.4Mo-0.45Si, Metall. Mater. Trans. A. 27 (1996) 1709–1717. doi:10.1007/BF02649829.
[20] W. Jia, W. Zeng, X. Zhang, Y. Zhou, J. Liu, Q. Wang, Oxidation behavior and effect of oxidation on tensile properties of Ti60 alloy, J. Mater. Sci. 46 (2011) 1351–1358. doi:10.1007/s10853-010-4926-1.
[21] J.E. Shamblen, T.K. Redden, Air contamination and embrittlement of titanium alloys, in The science, Technology and Application of Titanium, Pergamon Press, London, 1968.
[22] R.N. Shenoy, J. Unnam, R.K. Clark, Oxidation and embrittlement of Ti-6Al-2Sn-4Zr-2Mo alloy, Oxid. Met. 26 (1986) 105–124.
[23] Z. Liu, G. Welsch, Effects of oxygen and heat treatment on the mechanical properties of alpha and beta titanium alloys, Metall. Trans. A. 19 (1988) 527–542. doi:10.1007/BF02649267.
[24] A. Rosen, A. Rottem, The effect of high temperature exposure on the creep resistance of Ti-6Al-4V alloy, Mater. Sci. Eng. 22 (1976) 23–29. doi:10.1016/0025-5416(76)90132-4.
[25] R.W. Evans, R.J. Hull, B. Wilshire, The effects of alpha-case formation on the creep fracture properties of the high-temperature titanium alloy IMI834, J. Mater. Process. Technol. 56 (1996) 492–501. doi:10.1016/0924-0136(96)85109-0.
[26] A. Dubertret, PhD Thesis, Faculté des Sciences, Paris, 1970.
[27] M. Berthaud, PhD Thesis, Etude du comportement de l'alliage de titane Ti6242S à haute température sous atmosphères complexes : applications aéronautiques, Université de Bourgogne Franche-Comté, 2018.
[28] J. Baillieux, D. Poquillon, B. Malard, Relationship between the volume of the unit cell of hexagonal-close-packed Ti, hardness and oxygen content after α-case formation in Ti–6Al–2Sn–4Zr–2Mo–0.1 Si alloy, J. Appl. Crystallogr. 49 (2016) 175–181.
[29] R. Gaddam, B. Sefer, R. Pederson, M.-L. Antti, Oxidation and alpha-case formation in Ti–6Al–2Sn–4Zr–2Mo alloy, Mater. Charact. 99 (2015) 166–174. doi:10.1016/j.matchar.2014.11.023.
[30] H. Guleryuz, H. Cimenoglu, Oxidation of Ti–6Al–4V alloy, J. Alloys Compd. 472 (2009) 241–246. doi:10.1016/j.jallcom.2008.04.024.
[31] A.I. Kahveci, G.E. Welsch, Effect of oxygen on the hardness and alpha/beta phase ratio of Ti-6Al-4V alloy, Scr. Metall. 20 (1986) 1287–1290. doi:10.1016/0036-9748(86)90050-5.
[32] B. Champin, L. Graff, M. Armand, G. Béranger, C. Coddet, Oxydation des alliages de titane au voisinage des températures d'utilisation dans les turbomoteurs, J. Common Met. 69 (1980) 163–183. doi:10.1016/0022-5088(80)90052-1.
[33] R. Gaddam, B. Sefer, R. Pederson, M.L. Antti, Study of alpha-case depth in Ti-6Al-2Sn-4Zr-2Mo and Ti-6Al-4V, IOP Conf. Ser. Mater. Sci. Eng. 48 (2013) 1–8. doi:10.1088/1757-899X/48/1/012002.
[34] J.P. Rivière, L. Pichon, M. Drouet, A. Galdikas, D. Poquillon, Silicon based oxidation-resistant coatings on Ti6242 alloy by dynamic ion mixing, Surf. Coat. Technol. 200 (2006) 5498–5504. doi:10.1016/j.surfcoat.2005.07.074.
[35] C. Dupressoire, A. Rouaix-Vande Put, P. Emile, C. Archambeau-Mirguet, R. Peraldi, D. Monceau, Effect of Nitrogen on the Kinetics of Oxide Scale Growth and of Oxygen Dissolution in the Ti6242S Titanium-Based Alloy, Oxid. Met. 87 (2017) 343–353. doi:10.1007/s11085-017-9729-1.
[36] A.M. Chaze, C. Coddet, The role of nitrogen in the oxidation behaviour of titanium and some binary alloys, J. Common Met. 124 (1986) 73–84. doi:10.1016/0022-5088(86)90478-9.

[37] L. Lutterotti, Total pattern fitting for the combined size–strain–stress–texture determination in thin film diffraction, Nucl. Instrum. Methods Phys. Res. Sect. B Beam Interact. Mater. At. 268 (2010) 334–340. doi:10.1016/j.nimb.2009.09.053.
[38] N.C. Popa, The (hkl) Dependence of Diffraction-Line Broadening Caused by Strain and Size for all Laue Groups in Rietveld Refinement, J. Appl. Crystallogr. 31 (1998) 176–180. doi:10.1107/S0021889897009795.
[39] W.B. Pearson, A Handbook of Lattice Spacings and Structures of Metals and Alloys, Pergamon Press, 1958.
[40] D. Monceau, B. Pieraggi, Determination of Parabolic Rate Constants from a Local Analysis of Mass-Gain Curves, Oxid. Met. 50 (1998) 477–493. doi:10.1023/A:1018860909826.
[41] A. Savitzky, M.J. Golay, Smoothing and differentiation of data by simplified least squares procedures., Anal. Chem. 36 (1964) 1627–1639.
[42] S. Thomas, P.M.A. Sherwood, Valence Band Spectra of Aluminum Oxides, Hydroxides, and Oxyhydroxides Interpreted by X a Calculations, Anal. Chem. 64 (1992) 2488–2495.
[43] A. Nylund, I. Olefjord, Surface analysis of oxidized aluminium. 1. Hydration of Al2O3 and decomposition of Al(OH)3 in a vacuum as studied by ESCA, Surf. Interface Anal. 21 (1994) 283–289. doi:10.1002/sia.740210504.
[44] J. Chastain, R.C. King, J.F. Moulder, Handbook of X-ray photoelectron spectroscopy: a reference book of standard spectra for identification and interpretation of XPS data, Physical Electronics Eden Prairie, MN, 1995.
[45] L. Vandenbulcke, D. Rats, M.I. De Barros, R. Benoît, R. Erre, P. Andreazza, Two-step process for improved diamond deposition on titanium alloys at moderate temperature, Appl. Phys. Lett. 72 (1998) 501–503. doi:10.1063/1.120797.
[46] P.-Y. Jouan, M.-C. Peignon, Ch. Cardinaud, G. Lempérière, Characterisation of TiN coatings and of the TiN/Si interface by X-ray photoelectron spectroscopy and Auger electron spectroscopy, Appl. Surf. Sci. 68 (1993) 595–603. doi:10.1016/0169-4332(93)90241-3.
[47] I.Ier. Strydom, S. Hofmann, The contribution of characteristic energy losses in the core-level X-ray photoelectron spectroscopy peaks of TiN and (Ti, Al)N studied by electron energy loss spectroscopy and X-ray photoelectron spectroscopy, J. Electron Spectrosc. Relat. Phenom. 56 (1991) 85–103. doi:10.1016/0368-2048(91)80007-H.
[48] E.C. Onyiriuka, Aluminum, Titanium Boride, and Nitride Films Sputter-Deposited from Multicomponent Alloy Targets Studied by XPS, Appl. Spectrosc. 47 (1993) 35–37.
[49] D.W. Smith, Inorganic Substances: A Prelude to the Study of Descriptive Inorganic Chemistry, Cambridge University Press, 1990.
[50] B. Sefer, PhD Thesis, Oxidation and Alpha–Case Phenomena in Titanium Alloys used in Aerospace Industry: Ti–6Al–2Sn–4Zr–2Mo and Ti–6Al–4V, Luleå Tekniska Universitet, 2014.
[51] P. Kofstad, P.B. Anderson, O.J. Krudtaa, Oxidation of titanium in the temperature range 800–1200°C, J. Common Met. 3 (1961) 89–97. doi:10.1016/0022-5088(61)90001-7.
[52] H.L. Du, P.K. Datta, D.B. Lewis, J.S. Burnell-Gray, Air oxidation behaviour of Ti-6Al-4V alloy between 650 and 850°, Corros. Sci. 36 (1994) 631–642. doi:10.1016/0010-938X(94)90069-8.
[53] J. Stringer, The oxidation of titanium in oxygen at high temperatures, Acta Metall. 8 (1960) 758–766. doi:10.1016/0001-6160(60)90170-X.
[54] M. Göbel, V.A.C. Haanappel, M.F. Stroosnijder, On the Determination of Diffusion Coefficients of Oxygen in One-Phase Ti (α-Ti) and Two-Phase Ti–4Nb (α- and β-Ti) by Micro-Hardness Measurements, Oxid. Met. 55 (2001) 137–151. doi:10.1023/A:1010333410938.
[55] M. Raffy, PhD Thesis, Ecole Nationale Supérieure de Chimie de Paris, 1981.
[56] D. David, G. Beranger, E.A. Garcia, A Study of the Diffusion of Oxygen in α-Titanium Oxidized in the Temperature Range 460°–700°C, J. Electrochem. Soc. 130 (1983) 1423–1426. doi:10.1149/1.2119966.
[57] A. Anttila, J. Räisänen, J. Keinonen, Diffusion of nitrogen in α-Ti, Appl. Phys. Lett. 42 (1983) 498–500. doi:10.1063/1.93981.
[58] A.P. Broumas, N.M. Degnan, M.L. Meier, Oxygen diffusion into titanium, in: NASA Conf. Publ., NASA; 1998, 2003: pp. 457–468.

[59] A.M. Chaze, C. Coddet, Influence of alloying elements on the dissolution of oxygen in the metallic phase during the oxidation of titanium alloys, J. Mater. Sci. 22 (1987) 1206–1214. doi:10.1007/BF01233110.
[60] H.A. Wriedt, J.L. Murray, The N-Ti (nitrogen-titanium) system, Bull. Alloy Phase Diagr. 8 (1987) 378–388.
[61] D. David, E.A. Garcia, X. Lucas, G. Beranger, Etude de la diffusion de l'oxygène dans le titane α oxyde entre 700°C et 950°C, J. Common Met. 65 (1979) 51–69. doi:10.1016/0022-5088(79)90152-8.

Figure captions:

Figure 1: (a) SEM surface image of raw Ti6242S alloy and (b) corresponding X-ray diffraction pattern

Figure 2: (a) TEM dark field image of the raw Ti6242S sample and corresponding electron diffraction patterns of α-phase (b) and β-phase (c)

Figure 3: Weight gain versus oxidation time after exposure during (a) 100 hours and (b) 10000 hours in dry air at 560°C

Figure 4: Cross-section SEM images of TI6242S samples aged in laboratory air at 560°C for 1000 hours (a), 6000 hours (b) and 10000 hours (c)

Figure 5: X-ray diffraction pattern acquired after oxidation of TI6242S in laboratory air at 560°C for 10000 hours

Figure 6: TEM image of Ti6242S sample oxidised for 300 hours in laboratory air at 560°C (a) and EDS-TEM profile acquired on Ti6242S sample oxidised for 300 hours in laboratory air at 560°C (b)

Figure 7: XPS profiles acquired on TI6242S sample oxidised for 100 hours in laboratory air at 560°C

Figure 8: XPS spectra obtained at the oxide/atmosphere interface in the regions corresponding to Al2p (a) and O1s (b) peaks

Figure 9: XPS spectrums obtained in the metal near the metal/oxide interface for Ti2p (a) and N1s peaks (b)

Figure 10: Oxygen and hardness profiles after (a) 1000 hours, (b) 3000 hours, (c) 6000 hours and (d) 10000 hours oxidation of Ti6242S at 560°C in laboratory air

Figure 11: Thickness of oxygen dissolution area against exposure time (a) and against square root of exposure time (b) in laboratory air at 560°C

Figure 12: XRD patterns acquired on Ti6242S samples before and after exposure in air at 560°C during different time dwells

Figure 13: Evolution of α-Ti6242S cell parameters with the oxidation time at 650°C in air

Figure 14: Variation with exposure time of the surface mass gains related to oxide scale growth and to oxygen dissolution in the metallic substrate during exposure in laboratory air at 560°C

Table 1: Chemical composition of Ti6242S alloy

Element	Al	Sn	Zr	Mo	Si	Ti
Content (wt. %)	6.0	2.0	4.0	2.0	0.1	Bal.
Content (at. %)	10.6	0.8	2.1	1.0	0.2	Bal.

Table 2: SEM-EDS analyses of α and β phases of Ti6242S alloy

Element	Ti	Al	Mo	Zr	Sn	Si
Alloy nominal composition (at.%)	84.6	11.1	0.7	2.3	0.9	0.4
Dark grey grains (α-phase) (at.%)	84.3	12.5	0.1	2.0	0.8	0.3
Light grey grains (β-phase) (at.%)	84.4	7.1	3.3	3.8	1.1	0.3

Table 3: Lattice parameters of hcp and CC phase of Ti6242S alloy and comparison with literature data on Ti6242 and pure Ti

		TEM	**Rietveld**	Malinov *et al.* [15]	Pure Ti [39]
α-phase (hcp) at 25°C	a (Å)	2.939	2.937	2.937	2.950
	c (Å)	4.674	4.686	4.687	4.683
	c/a	1.590	1.596	1.596	1.587
β-phase (bcc) at 25°C	a (Å)	3.260	3.261	3.254	3.307 (at 900°C)

Table 4: Oxide layer thicknesses for different oxidation times in laboratory air at 560°C

Oxidation time (h)	Layer thickness (nm)
1000	130
6000	550
10000	700

Table 5: Thickness of oxygen dissolution area for after exposure up to 10000 hours in laboratory air at 560°C

Oxidation time (h)	Oxygen dissolution depth (µm)
1000	22
3000	30
6000	39
10000	50

Table 6: Oxygen dissolution and oxide growth contribution to the total weight gain during exposure in laboratory air at 560°C

Exposure time (h)	Oxygen dissolution contribution (%)	Oxide growth contribution (%)
1000	87	13
3000	85	15
6000	81	19
10000	79	21

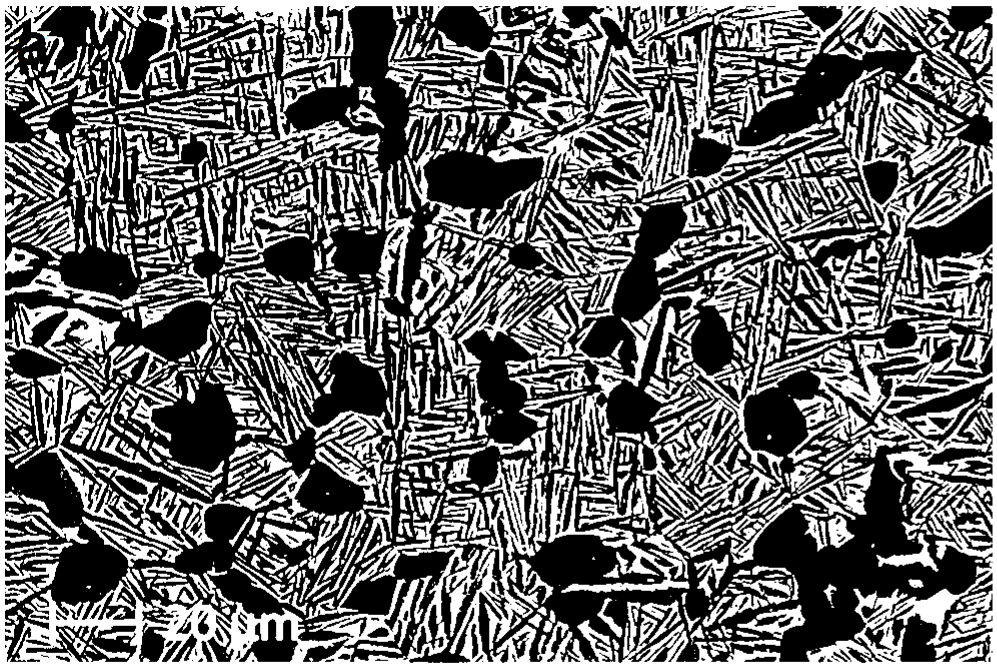
20 μm

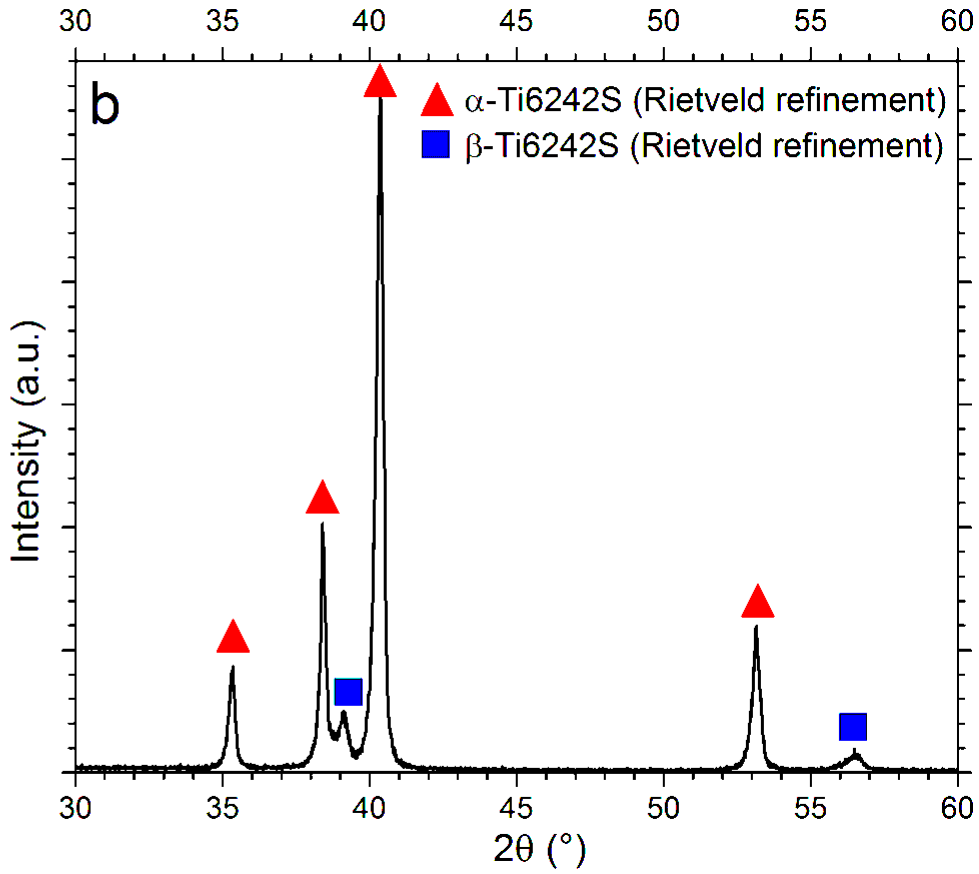
b
α-Ti6242S (Rietveld refinement)
β-Ti6242S (Rietveld refinement)
Intensity (a.u.)
2θ (°)
30
35
40
45
50
55
60

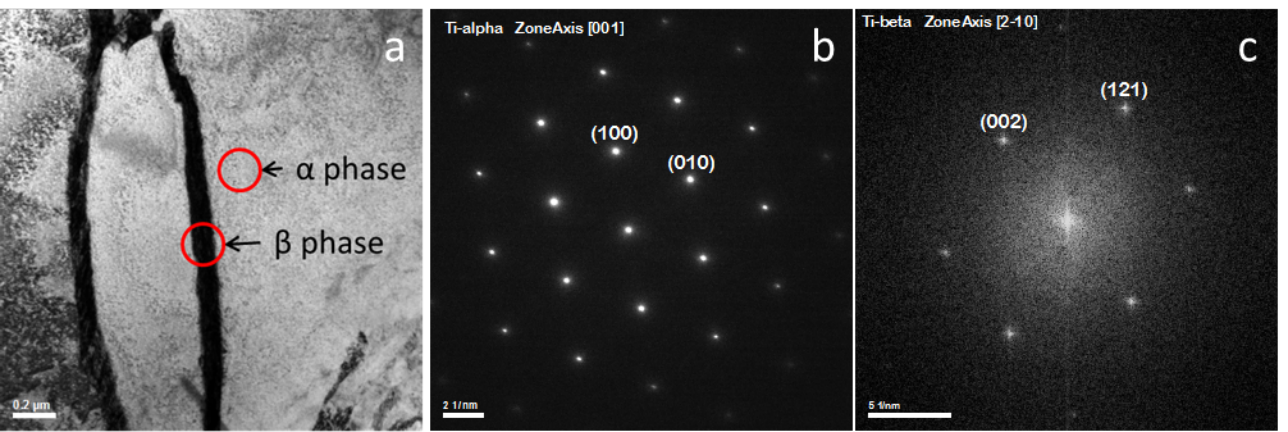
a
α phase
β phase
0.2 µm
Ti-alpha ZoneAxis [001]
b
(100)
(010)
2 1/nm
Ti-beta ZoneAxis [2-10]
c
(121)
(002)
5 1/nm

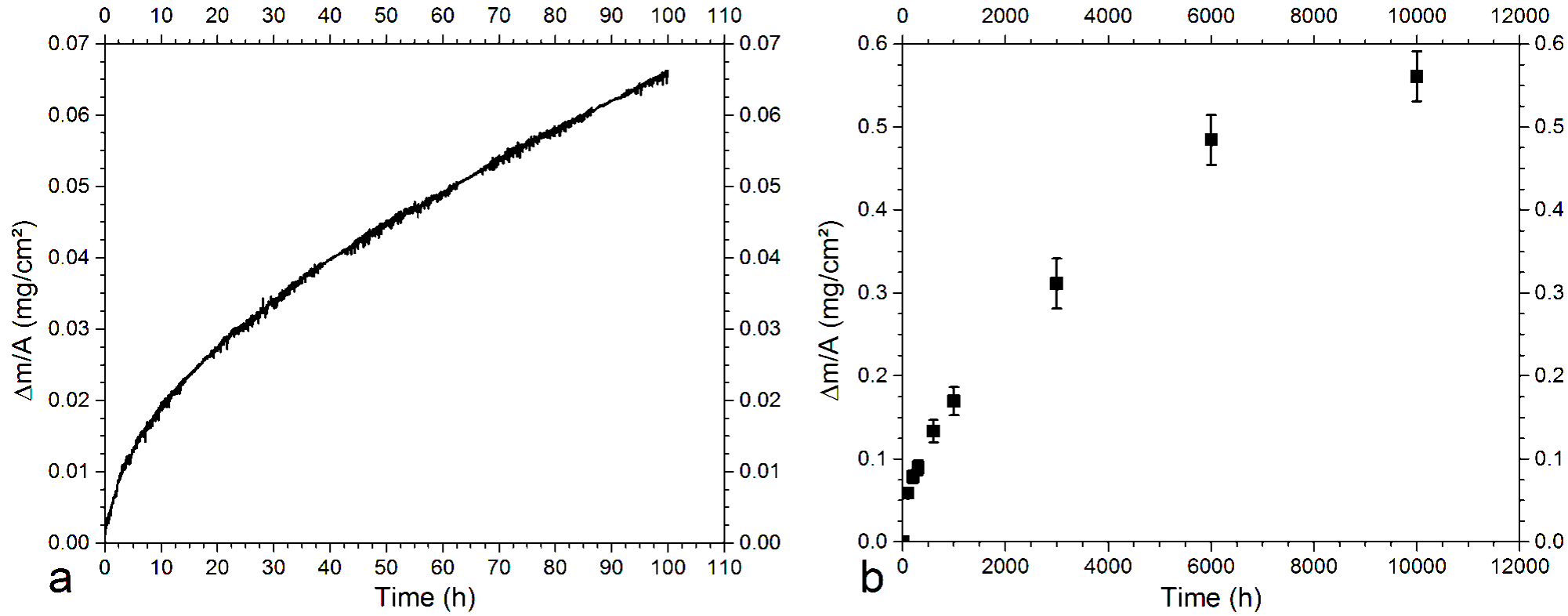
a
b
Δm/A (mg/cm²)
Time (h)
0
10
20
30
40
50
60
70
80
90
100
110
0.00
0.01
0.02
0.03
0.04
0.05
0.06
0.07
2000
4000
6000
8000
10000
12000
0.0
0.1
0.2
0.3
0.4
0.5
0.6

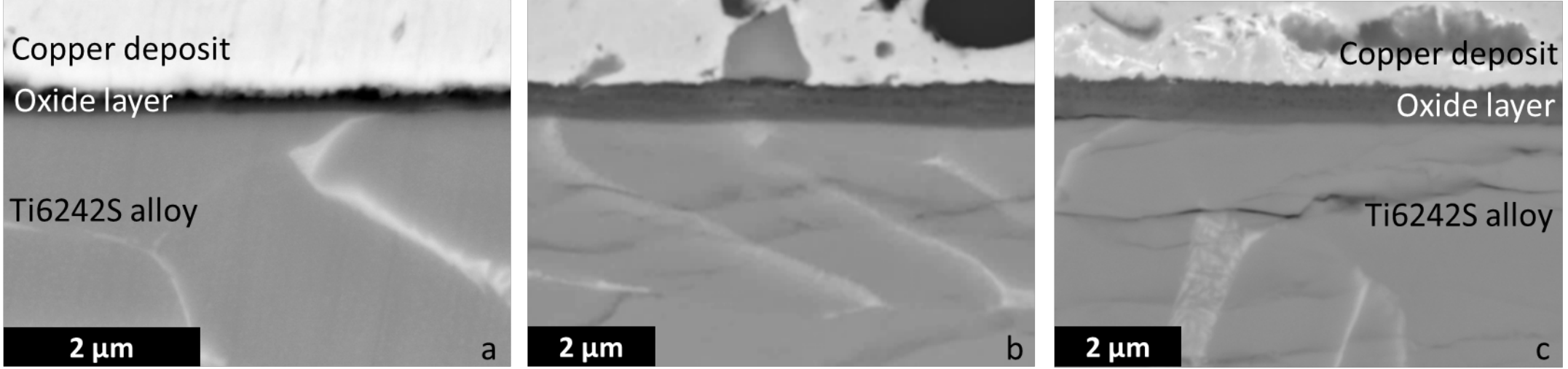
Copper deposit
Oxide layer
Ti6242S alloy
2 µm
a
2 µm
b
Copper deposit
Oxide layer
Ti6242S alloy
2 µm
c

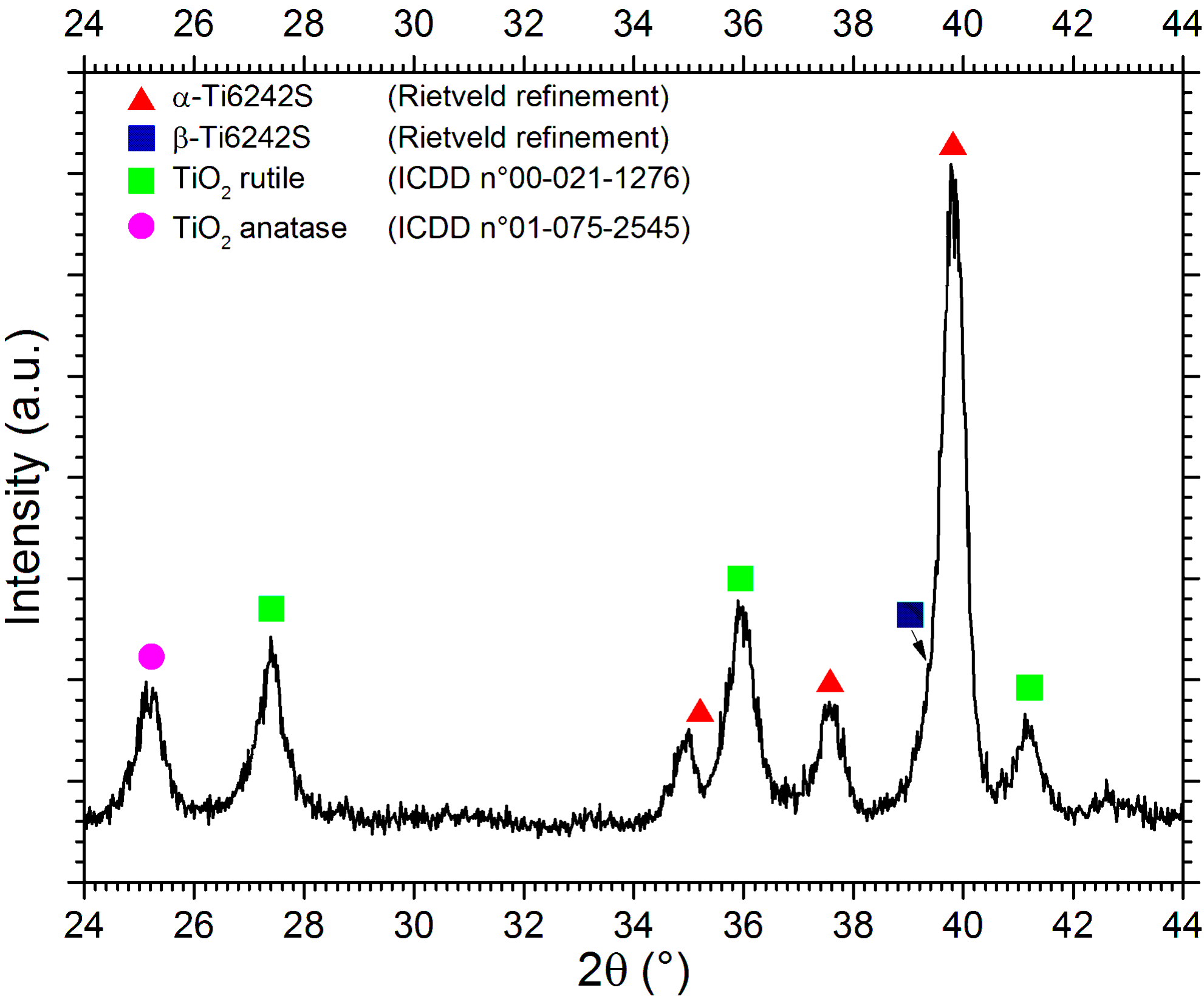
α-Ti6242S (Rietveld refinement)
β-Ti6242S (Rietveld refinement)
TiO2 rutile (ICDD n°00-021-1276)
TiO2 anatase (ICDD n°01-075-2545)
Intensity (a.u.)
2θ (°)
24
26
28
30
32
34
36
38
40
42
44

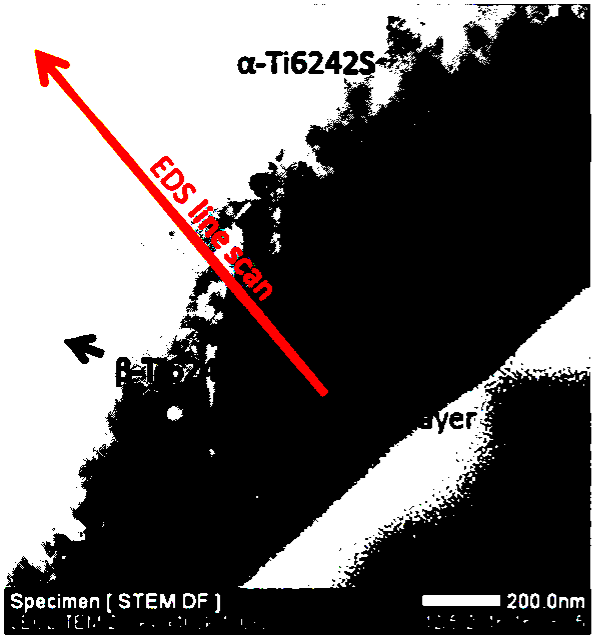
α-Ti6242S
EDS line scan
Specimen [STEM DF]
200.0nm

a

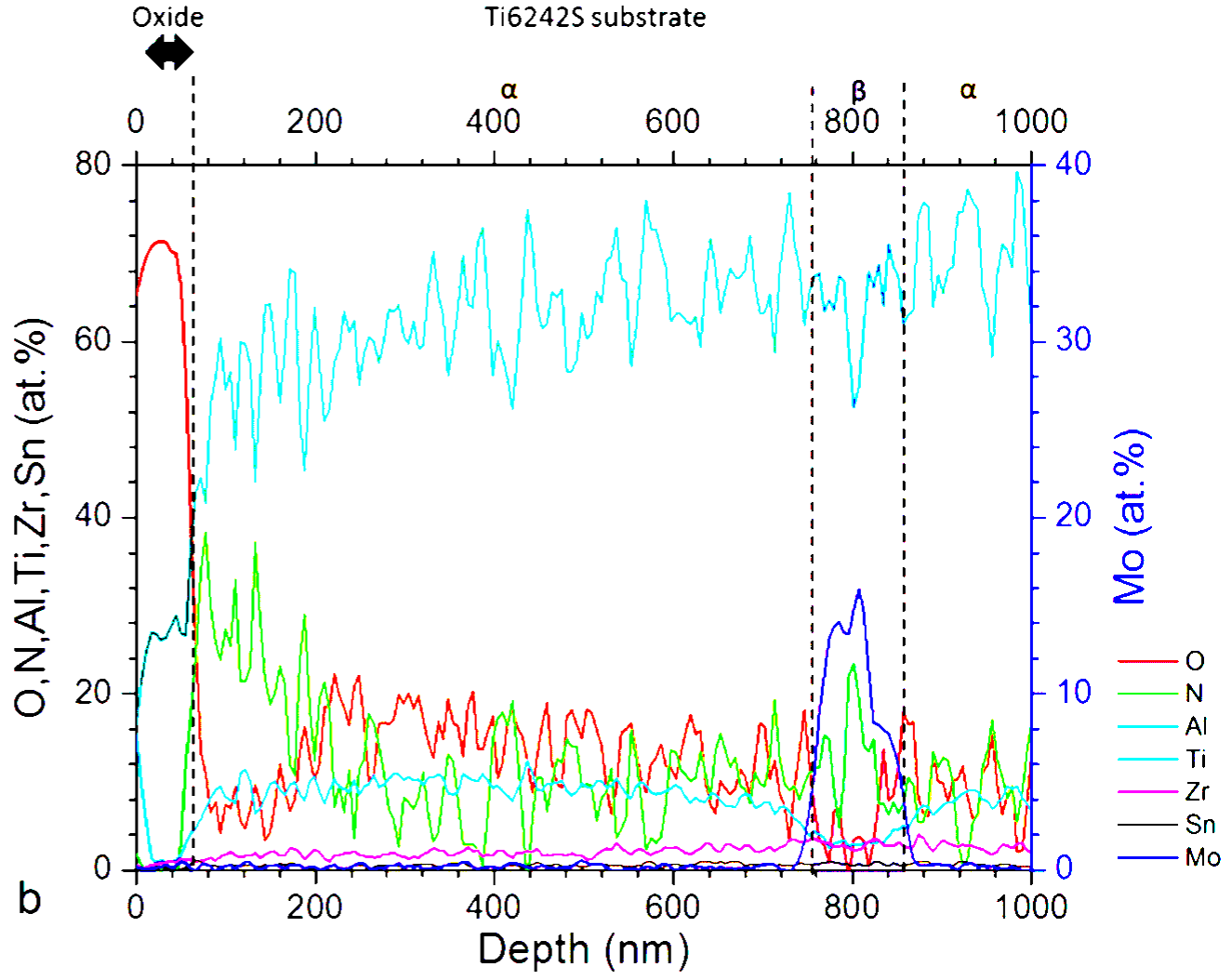
Oxide
Ti6242S substrate
α
β
α
0
200
400
600
800
1000
80
60
40
20
0
40
30
20
10
0
O,N,Al,Ti,Zr,Sn (at.%)
Mo (at.%)
Depth (nm)
O
N
Al
Ti
Zr
Sn
Mo

b

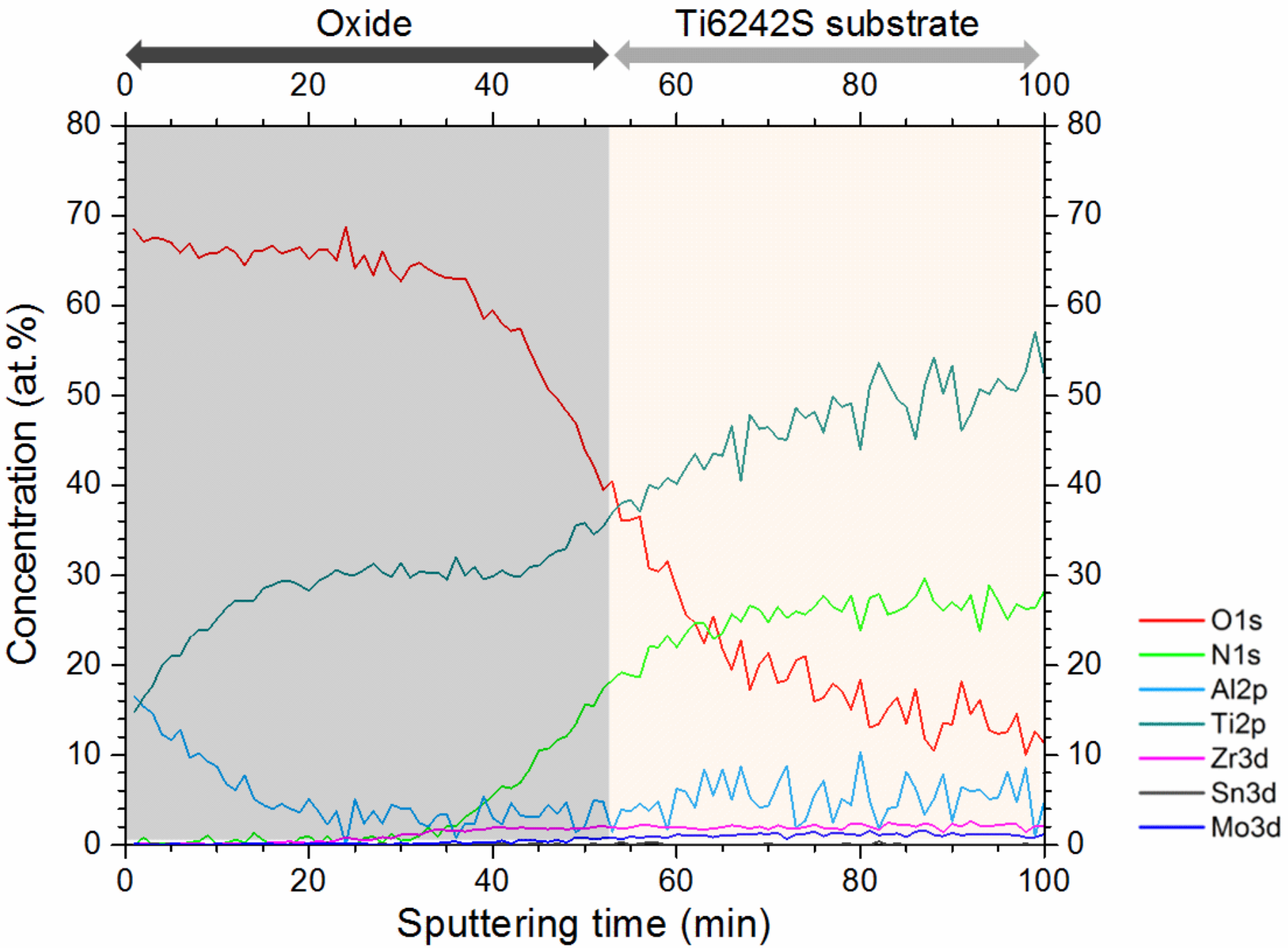
Oxide
Ti6242S substrate
0
20
40
60
80
100
Concentration (at.%)
Sputtering time (min)
O1s
N1s
Al2p
Ti2p
Zr3d
Sn3d
Mo3d

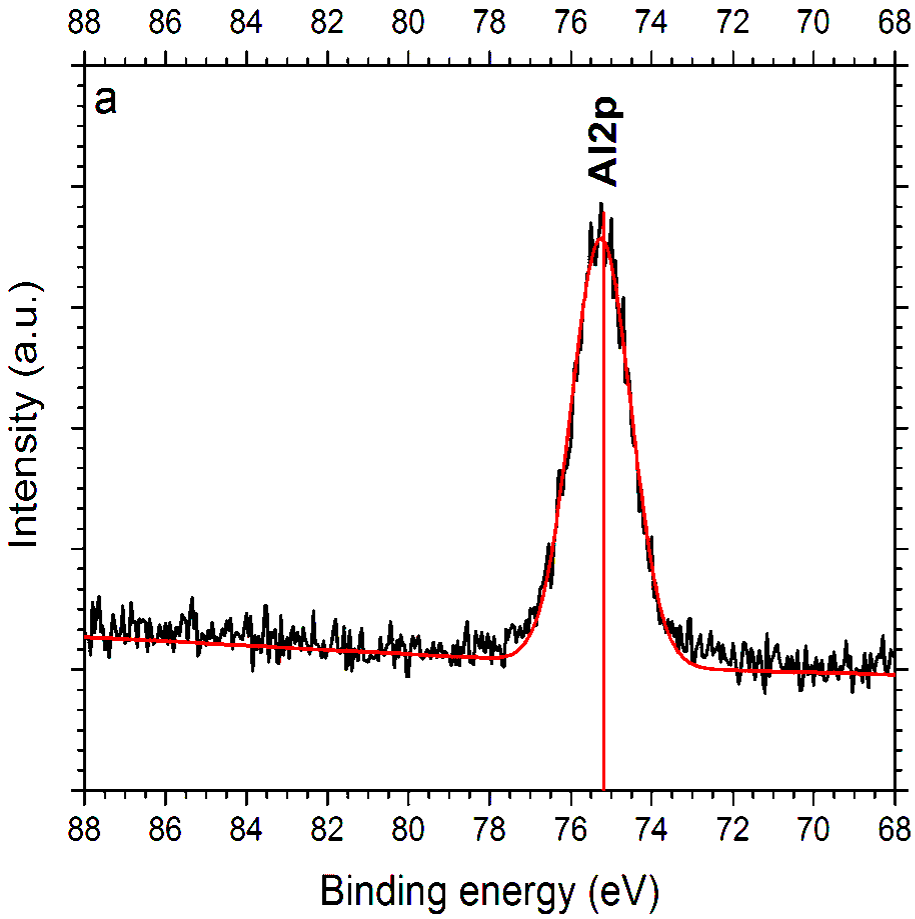
a
Al2p
Intensity (a.u.)
88 86 84 82 80 78 76 74 72 70 68
Binding energy (eV)

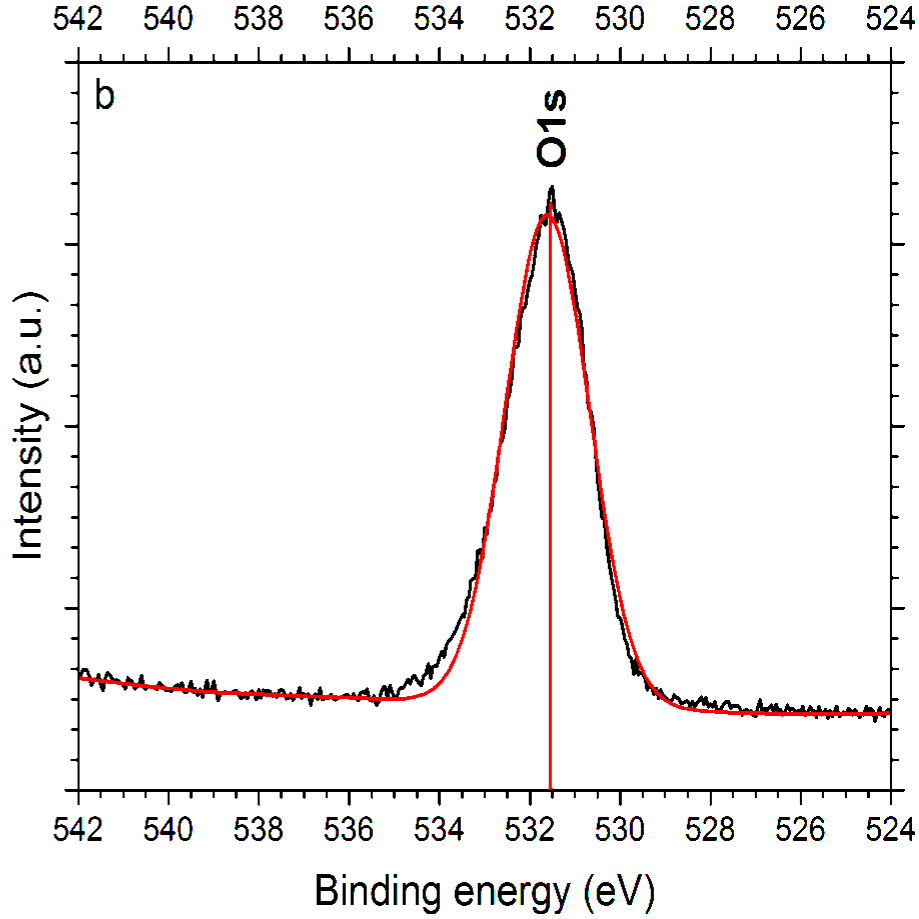
b
O1s
Intensity (a.u.)
542 540 538 536 534 532 530 528 526 524
Binding energy (eV)

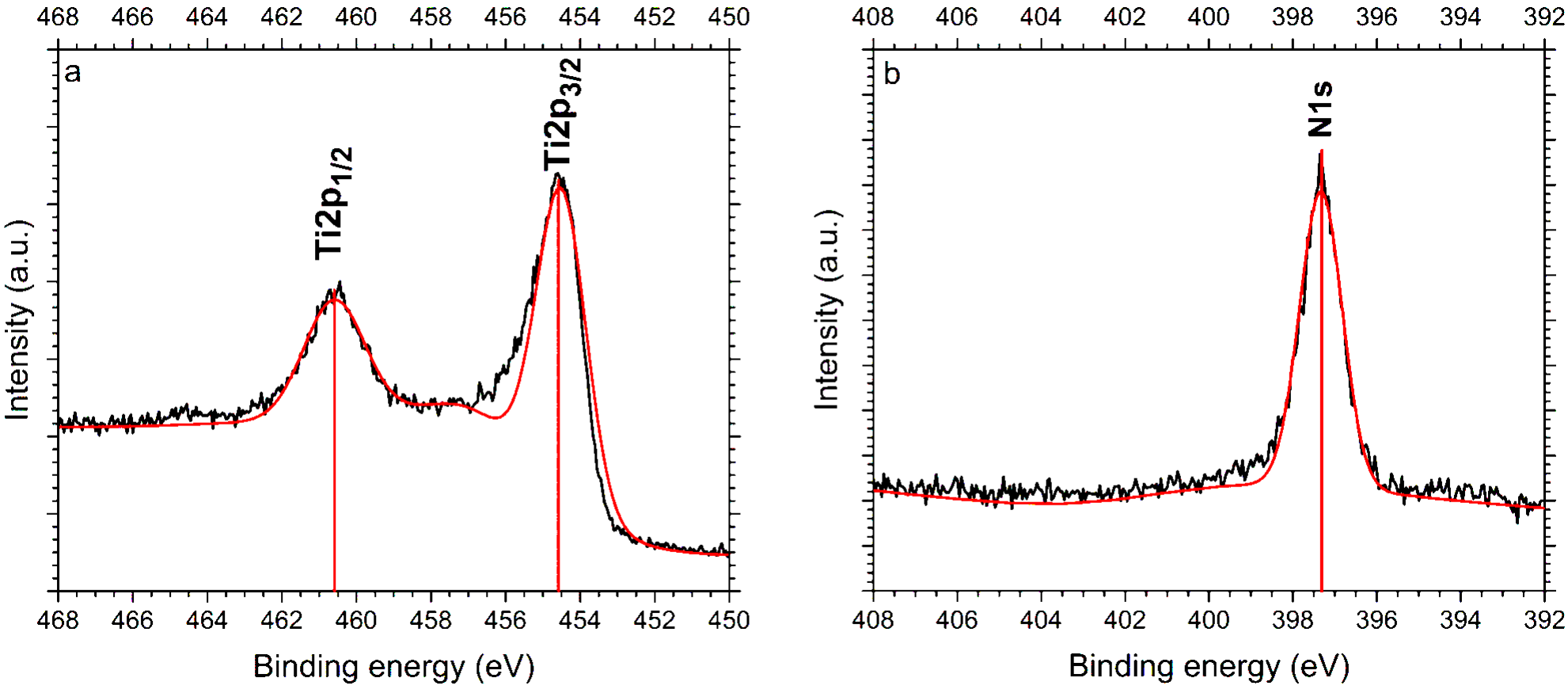
a
Ti2p1/2
Ti2p3/2
Intensity (a.u.)
Binding energy (eV)
468 466 464 462 460 458 456 454 452 450
b
N1s
Intensity (a.u.)
Binding energy (eV)
408 406 404 402 400 398 396 394 392

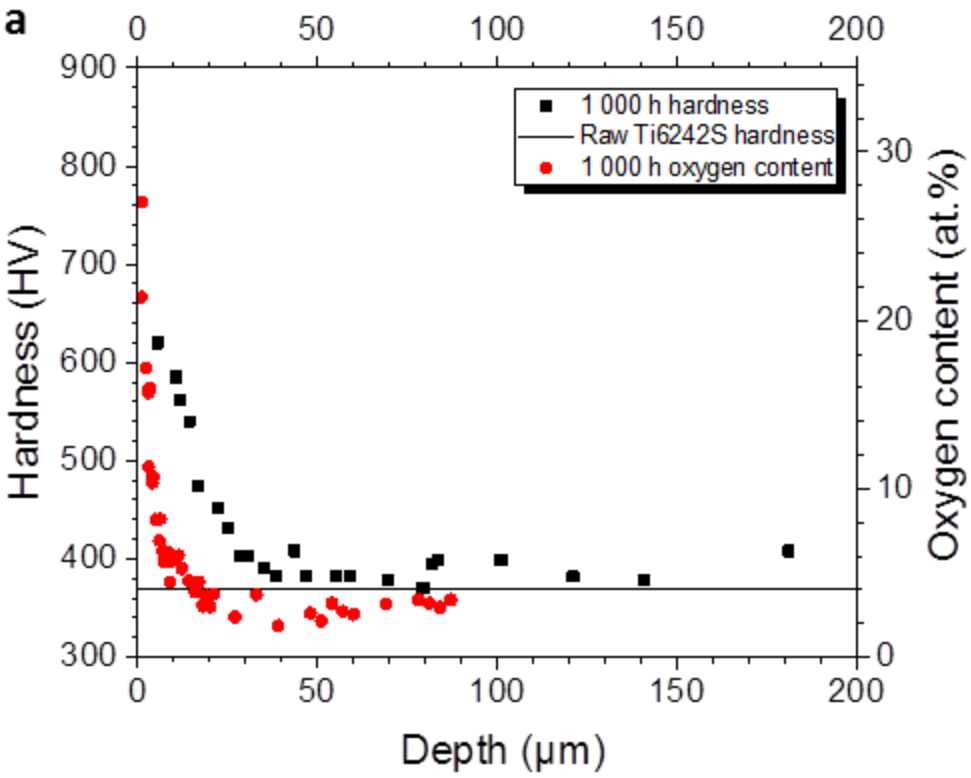
a
1 000 h hardness
Raw Ti6242S hardness
1 000 h oxygen content
Hardness (HV)
Oxygen content (at.%)
Depth (μm)

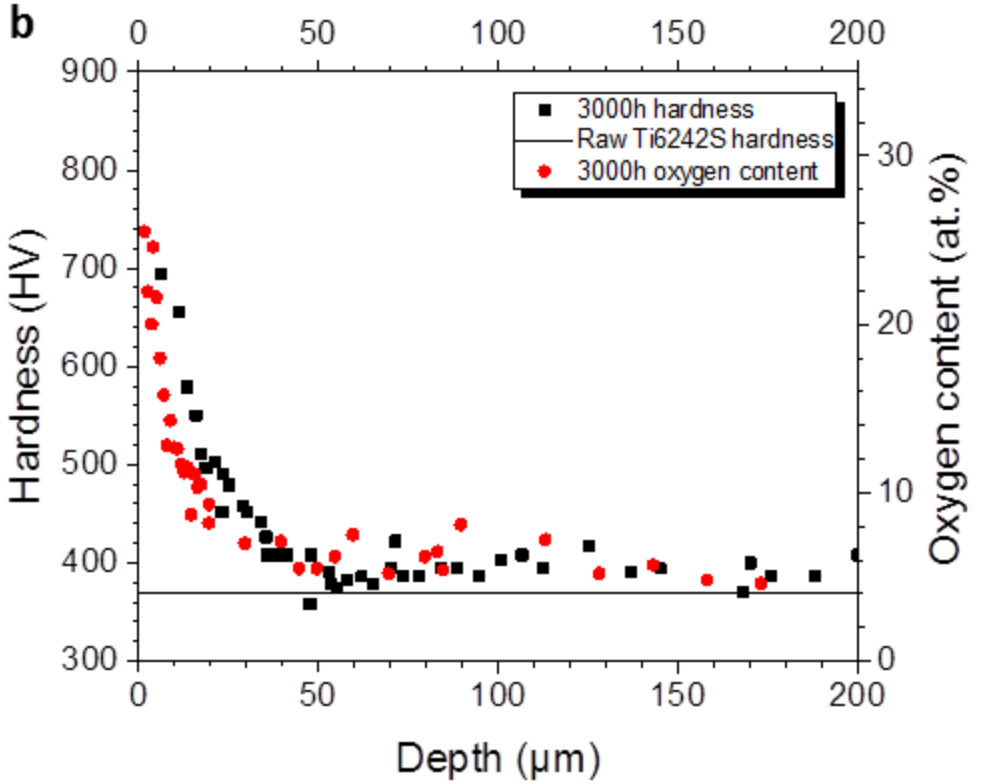
b
3000h hardness
Raw Ti6242S hardness
3000h oxygen content
Hardness (HV)
Oxygen content (at.%)
Depth (μm)

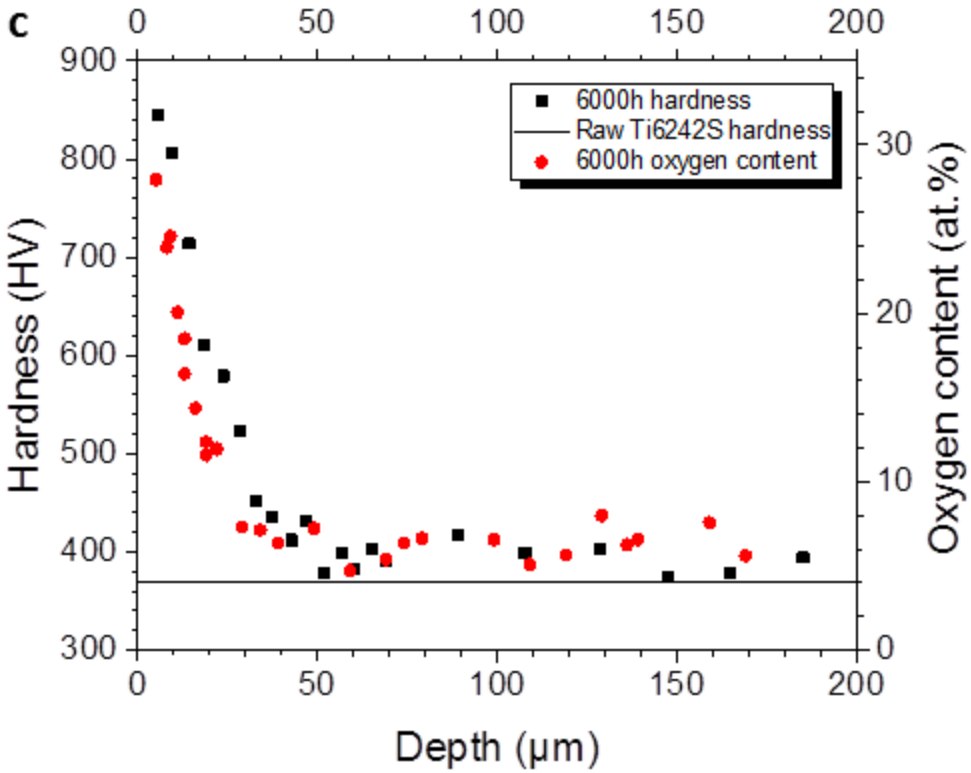
c
6000h hardness
Raw Ti6242S hardness
6000h oxygen content
Hardness (HV)
Oxygen content (at.%)
Depth (μm)

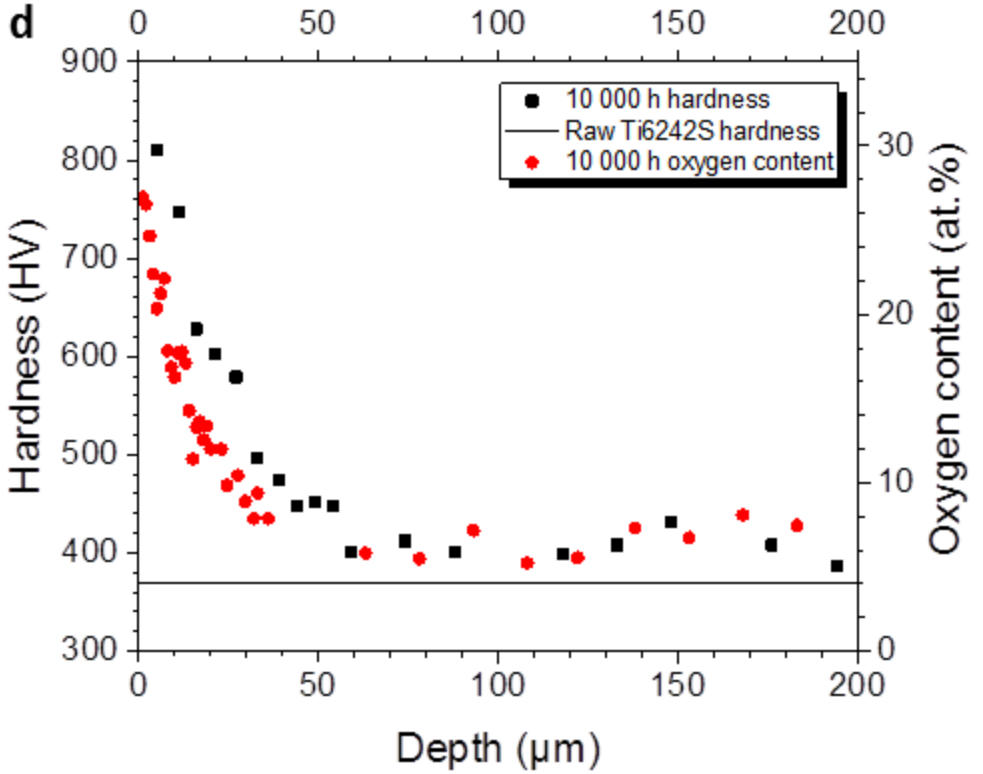
d
10 000 h hardness
Raw Ti6242S hardness
10 000 h oxygen content
Hardness (HV)
Oxygen content (at.%)
Depth (μm)

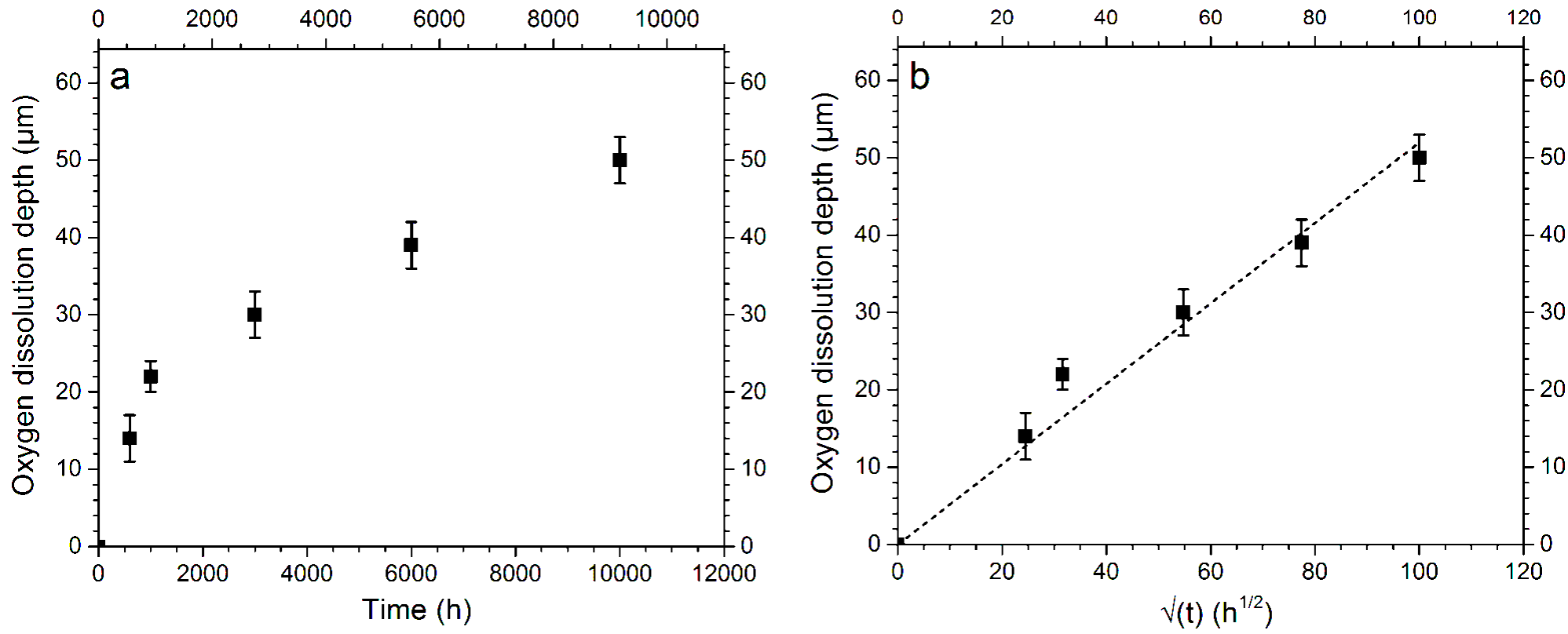
a
Oxygen dissolution depth (μm)
Time (h)
0
2000
4000
6000
8000
10000
12000
0
10
20
30
40
50
60
b
Oxygen dissolution depth (μm)
√(t) (h^1/2)
0
20
40
60
80
100
120

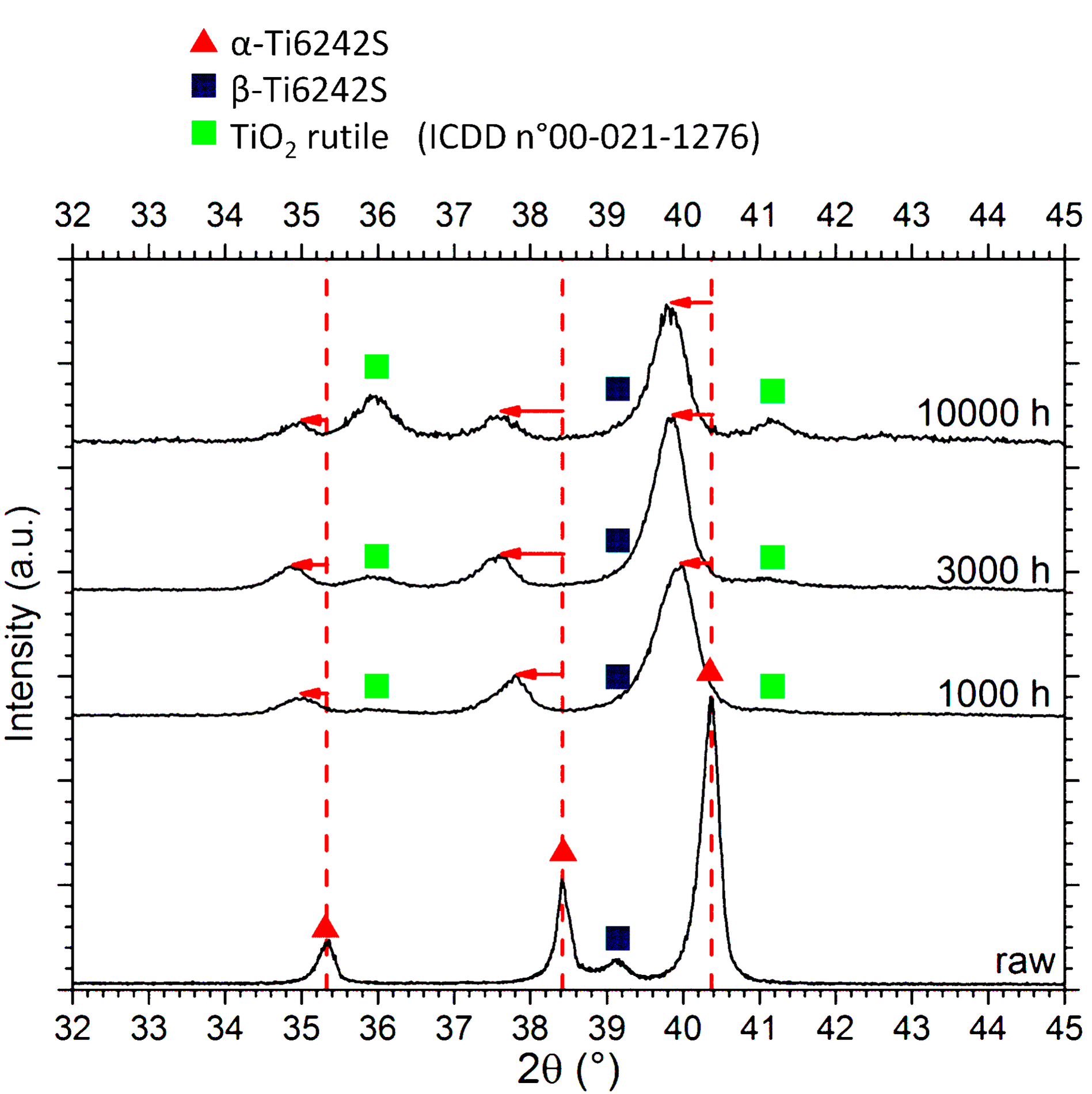
α-Ti6242S
β-Ti6242S
TiO2 rutile (ICDD n°00-021-1276)
32 33 34 35 36 37 38 39 40 41 42 43 44 45
10000 h
3000 h
1000 h
raw
Intensity (a.u.)
2θ (°)

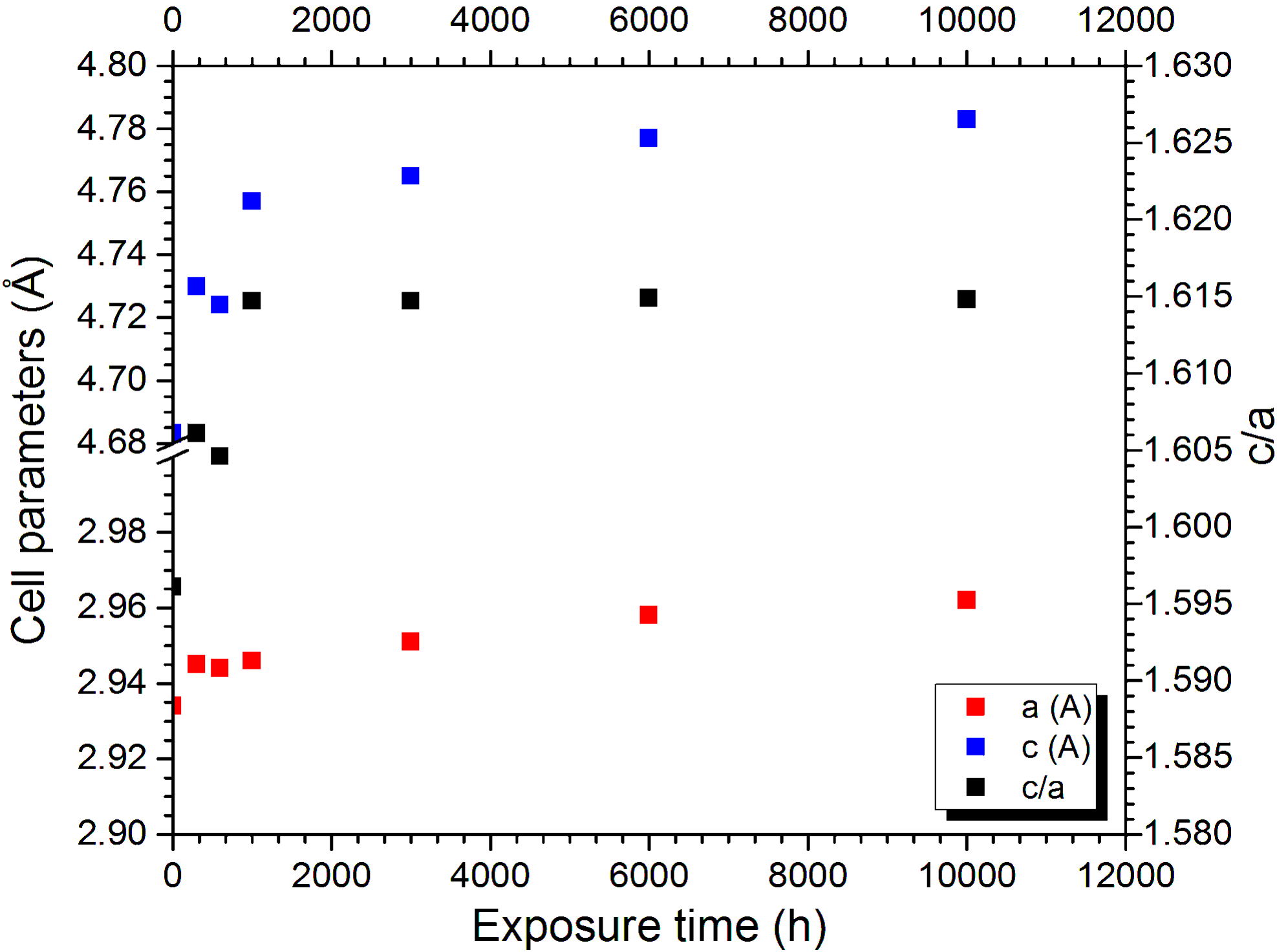
Cell parameters (Å)
c/a
Exposure time (h)
a (A)
c (A)
c/a
0
2000
4000
6000
8000
10000
12000
4.80
4.78
4.76
4.74
4.72
4.70
4.68
2.98
2.96
2.94
2.92
2.90
1.630
1.625
1.620
1.615
1.610
1.605
1.600
1.595
1.590
1.585
1.580

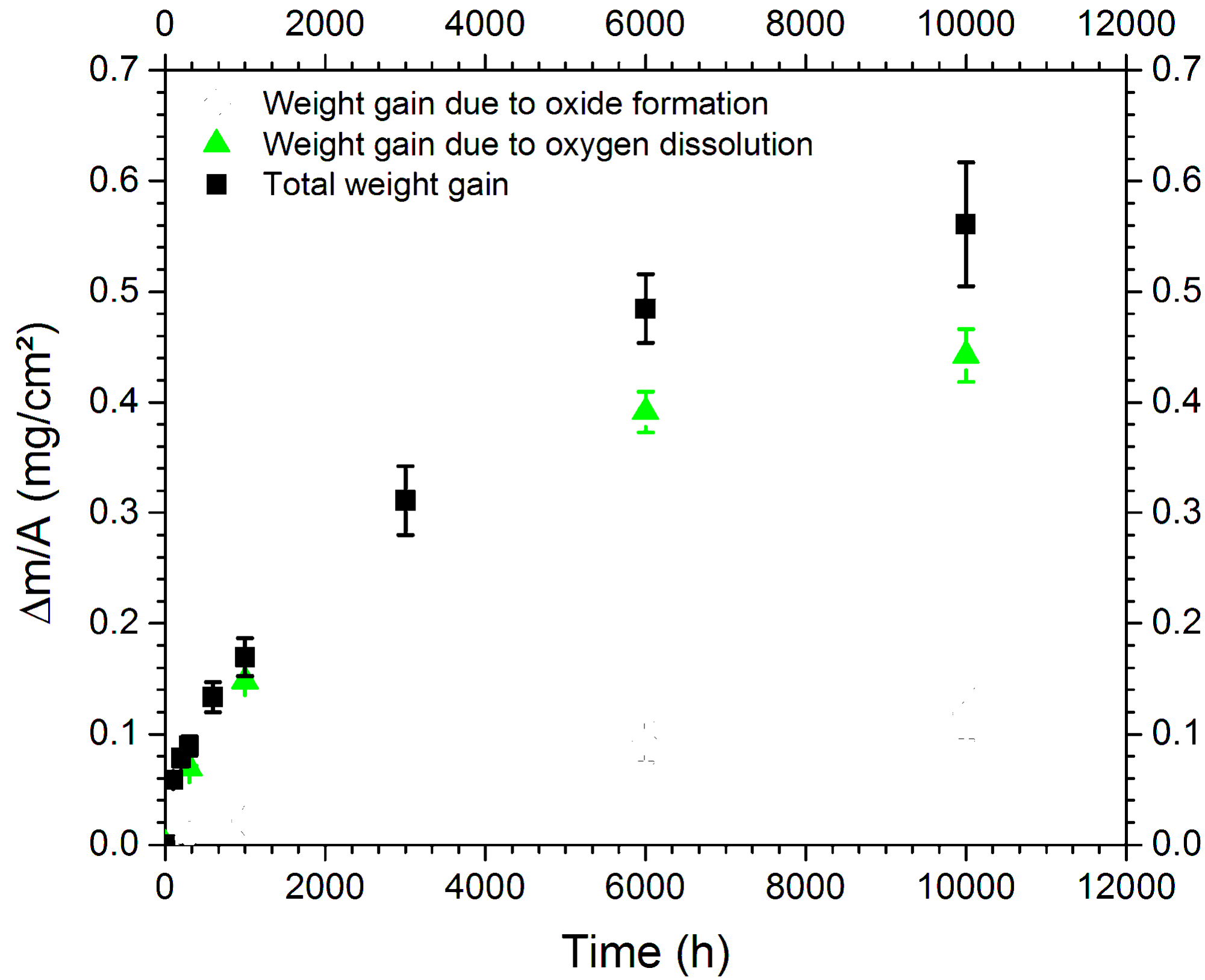
Weight gain due to oxide formation
Weight gain due to oxygen dissolution
Total weight gain
Δm/A (mg/cm²)
Time (h)
0
2000
4000
6000
8000
10000
12000
0.0
0.1
0.2
0.3
0.4
0.5
0.6
0.7